applications as well [23,24]. Therefore, the localization and biological effects of intranasally administered nanosilica particles must be elucidated. We expect that further studies of the relationship between localization and biological effects will provide useful information for the development of safer, effective NMs.

Conclusions

We have shown that nanosilica particles with diameters of 30, 70, and 100 nm intranasally administered to mice were absorbed into the bloodstream and distributed into certain organs, such as the liver. The obtained results suggest that the activation of an intrinsic cascade pathway induced by nanosilica particles with diameters of 30 and 70 nm, both of which activated coagulation factor XII and platelets, could result in abnormal activation of the coagulation system. We expect that the findings of this study will contribute to the ongoing development of NMs that are safe for use in humans and animals.

Methods

Silica particles

Amorphous nanosilica particles with diameters of 30, 70, and 100 nm, as well as microscale silica particles with diameters of 300 and 1000 nm (Micromod Partikeltechnologie, Rostock/Warnemünde, Germany, designated nSP30, nSP70, nSP100, mSP300, and mSP1000, respectively) were used in this study. The particle numbers of the silica particles were 3.5×10^{13}, 2.8×10^{12}, 9.5×10^{11}, 3.5×10^{10}, and 9.5×10^{8} particles/mg for nSP30, nSP70, nSP100, mSP300, and mSP1000, respectively. Each type of silica particles was sonicated for 5 min and vortexed for 1 min before use.

Animals

BALB/c mice (female, 6–8 weeks) were purchased from Japan SLC, Inc. (Shizuoka, Japan). Mice were housed in a ventilated animal room maintained at 20 ± 2°C with a 12-h light/12-h dark cycle. Mice had free access to water and alfalfa-free forage (FR-2, Funabashi Farm, Funabashi, Japan). All of the animal experimental procedures in this study were performed in accordance with the National Institute of Biomedical Innovation and Osaka University Guidelines for the Welfare of Animals.

Transmission electron microscopy analysis

Five BALB/c mice were intranasally exposed to a 20 μL aliquot (10 μL per nostril) of nSP30, nSP70, nSP100, mSP300, or mSP1000 at a concentration of 500 μg/mouse for 7 days. Twenty-four hours after the final intranasal administration, the nasal cavity, lung, and liver from two mice were excised and fixed in 2.5% glutaraldehyde for 2 h. Then, small pieces of tissue sample were washed with phosphate buffer 3 times and postfixed in sodium cacodylate-buffered 1.5% osmium tetroxide for 60 min at 4°C, block-stained in 0.5% uranyl acetate, dehydrated by dipping each sample through a series of ethanol solutions containing increasing concentration of ethanol, and embedded in Epon resin (TAAB). Ultrathin sections were stained with uranyl acetate and lead citrate. The stained samples were subsequently observed under an electron microscope (H-7650, Hitachi, Tokyo, Japan).

Histopathological examination

Twenty-four hours after the final intranasal administration of each type of silica particles, the nasal cavity, lung, and liver from three mice were excised and fixed immediately in 4% paraformaldehyde. These tissues were embedded in paraffin blocks and then sliced, and the slices were placed on glass slides. After hematoxylin–eosin staining, the slides were observed, and cell aggregation in the nasal cavity, microglial aggregation in the brain, and cell aggregation and rarefaction in the liver were classified into one of five grades (0: none, 1: very slight, 2: mild, 3: moderate, 4: advanced).

Blood biomarker assay

Twenty-four hours after the final intranasal administration of each type of silica particles, blood samples were collected from the heart using plastic syringes (Terumo, Tokyo, Japan) containing 5 IU/mL heparin sodium. Plasma was harvested by centrifuging the blood at 1750 × *g* for 15 min. The levels of ALT, ALB and BUN were determined in the plasma using a biochemical autoanalyzer (Fuji dri-Chem 7000, Fujifilm, Tokyo, Japan).

Hematology analysis

Twenty-four hours after the final intranasal administration of each type of amorphous silica particles, blood samples were collected from the heart using plastic syringes (Terumo) containing 0.1 mM EDTA. Whole blood samples were analyzed with a VetScan HMII Hematology System (Abaxis, Sunnyvale, CA, USA) to determine the number of white blood cells, lymphocytes, monocytes, and platelets.

Measurement of bleeding time and coagulation tests

Twenty-four hours after the final intranasal administration of each type of silica particles, the bleeding time for each mouse was measured by Duke's method [43]. Briefly, an ear of each mouse was cut with a knife, and the blood generated at the site of the cut was absorbed with filter paper every 30 seconds until bleeding ceased. To examine the coagulation tests in each mouse, a blood sample was collected from the heart of each mouse subjected to bleeding-time tests using plastic syringes (Terumo) containing 1:9 (v/v) of 3.8% sodium citrate. Plasma was harvested by

centrifuging the blood at 1750 × *g* for 15 min. APTT and PT levels were determined at 37°C in a Clotek dry-block bath system (Hyland Division, Travenol Laboratories, Inc. Costa Mesa, CA, USA) with APTT and PT reagents (Sysmex, Kobe, Japan), respectively.

In vitro activation tests of coagulation factor XII

One hundred microliters of human health plasma (Scipac, Kent, UK) and 100 μL of various sized silica particles (3.13 mg/mL) were mixed for 1 min at room temperature with an enzyme reaction solution (50 mM Tris–HCl, 0.15 M NaCl, 1 mM $CaCl_2$ and 0.1 mg/mL bovine serum albumin, pH 8.0) containing 2 mM *t*-butyloxycarbonyl-L-glutaminyl-glycyl-L-arginine-4-methyl-courmaryl-7-amide (Peptide Institute, Inc. Ibaraki, Japan) in dimethyl sulfoxide. The initial rate of reaction was calculated by measuring the fluorescence intensity (380 nm excitation, 440 nm emission) every 5 min. The initial rate is given by Initial rate = (relative fluorescent unit of each measurement time – blank) / measurement time.

Detection of TF, sCD40L, and vWF levels in plasma

TF, sCD40L, and vWF levels in plasma were determined using enzyme-linked immunosorbent assay (ELISA) kits (TF: Mouse Tissue Factor ELISA kit (Cusabio, Newark, DE, USA); sCD40L: Mouse sCD40L ELISA (eBioscience, San Diego, CA, USA); vWF: Mouse von Willebrand Factor ELISA kit (Cusabio, Newark, DE, USA)).

Statistical analysis

Differences among each group were compared by using Williams's or Dunnett's method after analysis of variance (ANOVA).

Competing interests

The authors declare that they have no competing interests.

Authors' contributions

TY and YY designed the study. TY, ST, TH, MU, and KI performed the experiments. TY and YY collected and analyzed the data. TY and YY wrote the manuscript. KN, YA, HK, ST, HN, KH, and TY provided technical support and conceptual advice. YT supervised the project. All authors discussed the results and commented on the manuscript. All authors read and approved the final manuscript.

Acknowledgements

This study was supported, in part, by Grants-in-Aid for Scientific Research from the Ministry of Education, Culture, Sports, Science and Technology of Japan (MEXT) and from the Japan Society for the Promotion of Science (JSPS); and by the Knowledge Cluster Initiative (MEXT); by Health Labour Sciences Research Grants from the Ministry of Health, Labour and Welfare of Japan (MHLW); by a Global Environment Research Fund from the Ministry of the Environment; by Food Safety Commission (Cabinet Office); by The Cosmetology Research Foundation; by The Smoking Research Foundation; by The Research Foundation for Pharmaceutical Sciences; and by The Takeda Science Foundation.

Author details

[1]Laboratory of Toxicology and Safety Science, Graduate School of Pharmaceutical Sciences, Osaka University, 1-6 Yamadaoka, Suita, Osaka 565-0871, Japan. [2]Laboratory of Biopharmaceutical Research, National Institute of Biomedical Innovation, 7-6-8 Saitoasagi, Ibaraki, Osaka 567-0085, Japan. [3]Cancer Biology Research Center, Sanford Research/USD, 2301 E. 60th Street N, Sioux Falls SD 57104, USA. [4]The Center for Advanced Medical Engineering and Informatics, Osaka University, 1-6 Yamadaoka, Suita, Osaka 565-0871, Japan. [5]Division of Foods, National Institute of Health Sciences, 1-18-1, Kamiyoga, Setagaya-ku, Tokyo 158-8501, Japan.

Received: 14 February 2013 Accepted: 14 August 2013
Published: 20 August 2013

References

1. Sozer N, Kokini JL: **Nanotechnology and its applications in the food sector.** *Trends Biotechnol* 2009, **27:**82–89.
2. McNeil SE: **Unique benefits of nanotechnology to drug delivery and diagnostics.** *Methods Mol Biol* 2011, **697:**3–8.
3. Sonkaria S, Ahn SH, Khare V: **Nanotechnology and its impact on food and nutrition: a review.** *Recent Pat Food Nutr Agric* 2012, **4:**8–18.
4. Knopp D, Tang D, Niessner R: **Review: bioanalytical applications of biomolecule-functionalized nanometer-sized doped silica particles.** *Anal Chim Acta* 2009, **647:**14–30.
5. Maynard AD, Aitken RJ, Butz T, Colvin V, Donaldson K, Oberdorster G, Philbert MA, Ryan J, Seaton A, Stone V, *et al*: **Safe handling of nanotechnology.** *Nature* 2006, **444:**267–269.
6. Kuhlbusch TA, Asbach C, Fissan H, Gohler D, Stintz M: **Nanoparticle exposure at nanotechnology workplaces: a review.** *Part Fibre Toxicol* 2011, **8:**22.
7. Donaldson K, Poland CA: **Inhaled nanoparticles and lung cancer - what we can learn from conventional particle toxicology.** *Swiss Med Wkly* 2012, **142:**w13547.
8. Poland CA, Duffin R, Kinloch I, Maynard A, Wallace WA, Seaton A, Stone V, Brown S, Macnee W, Donaldson K: **Carbon nanotubes introduced into the abdominal cavity of mice show asbestos-like pathogenicity in a pilot study.** *Nat Nanotechnol* 2008, **3:**423–428.
9. Hougaard KS, Jackson P, Jensen KA, Sloth JJ, Loschner K, Larsen EH, Birkedal RK, Vibenholt A, Boisen AM, Wallin H, *et al*: **Effects of prenatal exposure to surface-coated nanosized titanium dioxide (UV-Titan): a study in mice.** *Part Fibre Toxicol* 2010, **7:**16.
10. Morishige T, Yoshioka Y, Tanabe A, Yao X, Tsunoda S, Tsutsumi Y, Mukai Y, Okada N, Nakagawa S: **Titanium dioxide induces different levels of IL-1beta production dependent on its particle characteristics through caspase-1 activation mediated by reactive oxygen species and cathepsin B.** *Biochem Biophys Res Commun* 2010, **392:**160–165.
11. Nabeshi H, Yoshikawa T, Matsuyama K, Nakazato Y, Matsuo K, Arimori A, Isobe M, Tochigi S, Kondoh S, Hirai T, *et al*: **Systemic distribution, nuclear entry and cytotoxicity of amorphous nanosilica following topical application.** *Biomaterials* 2011, **32:**2713–2724.
12. Yamashita K, Yoshioka Y, Higashisaka K, Mimura K, Morishita Y, Nozaki M, Yoshida T, Ogura T, Nabeshi H, Nagano K, *et al*: **Silica and titanium dioxide nanoparticles cause pregnancy complications in mice.** *Nat Nanotechnol* 2011, **6:**321–328.
13. Yoshida T, Yoshioka Y, Fujimura M, Yamashita K, Higashisaka K, Morishita Y, Kayamuro H, Nabeshi H, Nagano K, Abe Y, *et al*: **Promotion of allergic immune responses by intranasally-administrated nanosilica particles in mice.** *Nanoscale Res Lett* 2011, **6:**195.
14. Hirai T, Yoshikawa T, Nabeshi H, Yoshida T, Tochigi S, Ichihashi K, Uji M, Akase T, Nagano K, Abe Y, *et al*: **Amorphous silica nanoparticles size-dependently aggravate atopic dermatitis-like skin lesions following an intradermal injection.** *Part Fibre Toxicol* 2012, **9:**3.
15. Nabeshi H, Yoshikawa T, Matsuyama K, Nakazato Y, Arimori A, Isobe M, Tochigi S, Kondoh S, Hirai T, Akase T, *et al*: **Amorphous nanosilicas induce consumptive coagulopathy after systemic exposure.** *Nanotechnology* 2012, **23:**045101.
16. Morishige T, Yoshioka Y, Inakura H, Tanabe A, Narimatsu S, Yao X, Monobe Y, Imazawa T, Tsunoda S, Tsutsumi Y, *et al*: **Suppression of nanosilica particle-induced inflammation by surface modification of the particles.** *Arch Toxicol* 2012, **86:**1297–1307.
17. Norris LA: **Blood coagulation.** *Best Pract Res Clin Obstet Gynaecol* 2003, **17:**369–383.
18. Zhuo R, Miller R, Bussard KM, Siedlecki CA, Vogler EA: **Procoagulant stimulus processing by the intrinsic pathway of blood plasma coagulation.** *Biomaterials* 2005, **26:**2965–2973.

19. Muller F, Renne T: **Platelet polyphosphates: the nexus of primary and secondary hemostasis.** *Scand J Clin Lab Invest* 2011, **71**:82–86.
20. Blann AD: **Plasma von Willebrand factor, thrombosis, and the endothelium: the first 30 years.** *Thromb Haemost* 2006, **95**:49–55.
21. Pamukcu B, Lip GY, Snezhitskiy V, Shantsila E: **The CD40-CD40L system in cardiovascular disease.** *Ann Med* 2011, **43**:331–340.
22. Merget R, Bauer T, Kupper HU, Philippou S, Bauer HD, Breitstadt R, Bruening T: **Health hazards due to the inhalation of amorphous silica.** *Arch Toxicol* 2002, **75**:625–634.
23. Moghimi SM, Hunter AC, Murray JC: **Nanomedicine: current status and future prospects.** *FASEB J* 2005, **19**:311–330.
24. Slowing II, Vivero-Escoto JL, Wu CW, Lin VS: **Mesoporous silica nanoparticles as controlled release drug delivery and gene transfection carriers.** *Adv Drug Deliv Rev* 2008, **60**:1278–1288.
25. Warheit DB, Carakostas MC, Kelly DP, Hartsky MA: **Four-week inhalation toxicity study with Ludox colloidal silica in rats: pulmonary cellular responses.** *Fundam Appl Toxicol* 1991, **16**:590–601.
26. Lee KP, Kelly DP: **The pulmonary response and clearance of Ludox colloidal silica after a 4-week inhalation exposure in rats.** *Fundam Appl Toxicol* 1992, **19**:399–410.
27. Sonaje K, Lin KJ, Tseng MT, Wey SP, Su FY, Chuang EY, Hsu CW, Chen CT, Sung HW: **Effects of chitosan-nanoparticle-mediated tight junction opening on the oral absorption of endotoxins.** *Biomaterials* 2011, **32**:8712–8721.
28. Vllasaliu D, Exposito-Harris R, Heras A, Casettari L, Garnett M, Illum L, Stolnik S: **Tight junction modulation by chitosan nanoparticles: comparison with chitosan solution.** *Int J Pharm* 2010, **400**:183–193.
29. Wang J, Chen C, Liu Y, Jiao F, Li W, Lao F, Li Y, Li B, Ge C, Zhou G, *et al*: **Potential neurological lesion after nasal instillation of TiO(2) nanoparticles in the anatase and rutile crystal phases.** *Toxicol Lett* 2008, **183**:72–80.
30. Wang J, Liu Y, Jiao F, Lao F, Li W, Gu Y, Li Y, Ge C, Zhou G, Li B, *et al*: **Time-dependent translocation and potential impairment on central nervous system by intranasally instilled TiO(2) nanoparticles.** *Toxicology* 2008, **254**:82–90.
31. Liu Y, Gao Y, Zhang L, Wang T, Wang J, Jiao F, Li W, Liu Y, Li Y, Li B, *et al*: **Potential health impact on mice after nasal instillation of nano-sized copper particles and their translocation in mice.** *J Nanosci Nanotechnol* 2009, **9**:6335–6343.
32. Kim SF, Daniel JW, Francois LP, Anwen MKH, Hui QL, John VH, Barbé CJ: **Biodegradability of sol–gel silica microparticles for drug delivery.** *Journal of Sol-gel Science and Technology* 2009, **49**:12–18.
33. Zhai W, He C, Wu L, Zhou Y, Chen H, Chang J, Zhang H: **Degradation of hollow mesoporous silica nanoparticles in human umbilical vein endothelial cells.** *J Biomed Mater Res B Appl Biomater* 2012, **100**:1397–1403.
34. He Q, Shi J, Zhu M, Chen Y, Chen F: **The three-stage *in vitro* degradation behavior of mesoporous silica in simulated body fluid.** *Microporous and Mesoporous Materials* 2010, **131**:314–320.
35. Bihari P, Holzer M, Praetner M, Fent J, Lerchenberger M, Reichel CA, Rehberg M, Lakatos S, Krombach F: **Single-walled carbon nanotubes activate platelets and accelerate thrombus formation in the microcirculation.** *Toxicology* 2010, **269**:148–154.
36. Burke AR, Singh RN, Carroll DL, Owen JD, Kock ND, D'Agostino R Jr, Torti FM, Torti SV: **Determinants of the thrombogenic potential of multiwalled carbon nanotubes.** *Biomaterials* 2011, **32**:5970–5978.
37. Meng J, Cheng X, Liu J, Zhang W, Li X, Kong H, Xu H: **Effects of long and short carboxylated or aminated multiwalled carbon nanotubes on blood coagulation.** *PLoS One* 2012, **7**:e38995.
38. Nemmar A, Melghit K, Ali BH: **The acute proinflammatory and prothrombotic effects of pulmonary exposure to rutile TiO2 nanorods in rats.** *Exp Biol Med (Maywood)* 2008, **233**:610–619.
39. Colman RW: **Surface-mediated defense reactions. The plasma contact activation system.** *J Clin Invest* 1984, **73**:1249–1253.
40. Colman RW, Schmaier AH: **Contact system: a vascular biology modulator with anticoagulant, profibrinolytic, antiadhesive, and proinflammatory attributes.** *Blood* 1997, **90**:3819–3843.
41. Tavano R, Segat D, Reddi E, Kos J, Rojnik M, Kocbek P, Iratni S, Scheglmann D, Colucci M, Echevarria IM, Selvestrel F, Mancin F, Papini E: **Procoagulant properties of bare and highly PEGylated vinyl-modified silica nanoparticles.** *Nanomedicine (Lond)* 2010, **5**:881–896.
42. Barik TK, Sahu B, Swain V: **Nanosilica-from medicine to pest control.** *Parasitol Res* 2008, **103**:253–258.
43. Angelkort B, Zilkens KW, Wenzel E: **Bleeding time (Duke) as a clinical function test of the primary phase of hemostasis.** *Med Welt* 1976, **27**:2302–2304.

doi:10.1186/1743-8977-10-41
Cite this article as: Yoshida *et al.*: Intranasal exposure to amorphous nanosilica particles could activate intrinsic coagulation cascade and platelets in mice. *Particle and Fibre Toxicology* 2013 **10**:41.

Journal of Thrombosis and Haemostasis, **11**: 1742–1750 DOI: 10.1111/jth.12355

ORIGINAL ARTICLE

RUNX1, but not its familial platelet disorder mutants, synergistically activates *PF4* gene expression in combination with ETS family proteins

Y. OKADA,*[1] M. WATANABE,†[1] T. NAKAI,* Y. KAMIKAWA,* M. SHIMIZU,* Y. FUKUHARA,* M. YONEKURA,* E. MATSUURA,* Y. HOSHIKA,* R. NAGAI,* W. C. AIRD‡ and T. DOI*†

*Graduate School of Pharmaceutical Sciences, Osaka University; †Graduate School of Frontier Biosciences, Osaka University, Osaka, Japan; and ‡Division of Molecular and Vascular Medicine, Center for Vascular Biology Research, Beth Israel Deaconess Medical Center, Boston, MA, USA

To cite this article: Okada Y, Watanabe M, Nakai T, Kamikawa Y, Shimizu M, Fukuhara Y, Yonekura M, Matsuura E, Hoshika Y, Nagai R, Aird WC, Doi T. *RUNX1*, but not its familial platelet disorder mutants, synergistically activates *PF4* gene expression in combination with ETS family proteins. *J Thromb Haemost* 2013; **11**: 1742–50.

Summary. *Background:* Familial platelet disorder (FPD) is a rare autosomal dominant disease characterized by thrombocytopenia and abnormal platelet function. Causal mutations have been identified in the gene encoding runt-related transcription factor 1 (*RUNX1*) of FPD patients. *Objectives:* To elucidate the role of *RUNX1* in the regulation of expression of platelet factor 4 (*PF4*) and to propose a plausible mechanism underlying *RUNX1*-mediated induction of the FPD phenotype. *Methods:* We assessed whether *RUNX1* and its mutants, in combination with E26 transformation-specific-1 (ETS-1), Core-binding factor subunit beta (CBFβ), and Friend leukemia virus integration 1 (FLI-1), cooperatively regulate *PF4* expression during megakaryocytic differentiation. In an embryonic stem cell differentiation system, expression levels of endogenous and exogenous *RUNX1* and *PF4* were determined by real-time RT-PCR. Promoter activation by the transcription factors were evaluated by reporter gene assays with HepG2 cells. DNA binding activity and protein interaction were analyzed by electrophoretic mobility shift assay and immunoprecipitation assay with Cos-7 cells, respectively. Protein localization was analyzed by immunocytochemistry and Western blotting with Cos-7 cells. *Results:* We demonstrated that *RUNX1* activates endogenous *PF4* expression in megakaryocytic differentiation. *RUNX1*, but not its mutants, in combination with ETS-1 and CBFβ, or FLI-1, synergistically activated the *PF4* promoter. Each RUNX1 mutant harbors various functional abnormalities, including loss of DNA-binding activity, abnormal subcellular localization, and/or alterations of binding affinities for ETS-1, CBFβ, and FLI-1. *Conclusions: RUNX1*, but not its mutants, strongly and synergistically activates *PF4* expression along with ETS family proteins. Furthermore, loss of the *RUNX1* transcriptional activation function is induced by various functional abnormalities.

Keywords: ETS1 protein, human; FLI1 protein, human; megakaryocytes; platelet disorder, familial, with associated myeloid malignancy; platelet factor 4; RUNX1 protein, human.

Correspondence: Yoshiaki Okada, Graduate School of Pharmaceutical Sciences, Osaka University, 1-6 Yamadaoka, Suita, Osaka 565-0871, Japan.
Tel.: +81 6 6879 8164; fax.: +81 6 6879 8164.
E-mail: okadabos@phs.osaka-u.ac.jp

[1]These authors equally contributed to this work.

Received 4 February 2013
Manuscript handled by: J. Heemskerk
Final decision: P. H. Reitsma, 27 June 2013

Introduction

Runt-related transcription factor 1 (RUNX1, also known as AML1 and CBFA2) is a key regulator of fetal and adult hematopoiesis. While studies on RUNX1-deficient mice have revealed that RUNX1 is essential for establishing definitive hematopoiesis during fetal development [1,2], RUNX1-conditional knockout mouse models have demonstrated its role in differentiation and maturation of megakaryocytes and lymphocytes in adults [3,4]. Thus, RUNX1 regulates the differentiation of hematopoietic cells into multilineages at multiple stages of development.

The cell type– and differentiation stage–specific RUNX1 functions are thought to be defined by its interacting factors. RUNX1 acts as both transcriptional activator and suppressor by interacting with various transcription factors and cofactors, such as CBFβ [4–6], GATA-1 [7], mSin3A [8], and ETS family proteins, ETS-1 [9] and FLI-1 [10]. For example, the interaction of

RUNX1 with ETS-1 augments its DNA-binding activity and enhances activation of T-cell receptor β gene expression [9], whereas its interaction with mSin3A suppresses *p21* gene expression [8]. In addition, RUNX1 changes binding partner during megakaryocytic differentiation and regulates gene expression in a differentiation stage–dependent manner [10,11]. This complicates investigation of the role of RUNX1 using leukemic cell lines, which cannot completely mimic physiological megakaryocytic differentiation.

In previous investigations of the mechanisms underlying megakaryocyte-specific gene expression, we identified several transcription factors, including ETS family proteins, ETS-1, FLI-1, and GABP, which regulate expression of platelet factor 4 (*PF4*), which is expressed specifically in megakaryocytes and platelets [12–15]. Furthermore, we demonstrated that RUNX1 suppresses megakaryocyte-specific genes, including *PF4*, in UT-7/GM cells treated with thrombopoietin (TPO) [16]. In contrast to our previous results, which demonstrated the potential role of RUNX1 as a suppressor of *PF4* expression in UT-7/GM cells, a study by Aneja *et al.* showed that RUNX1 activates the *PF4* expression in a megakaryocytic cell line, HEL cells [17]. In view of these ambiguous results, it remains unclear whether RUNX1 positively or negatively regulates *PF4* expression in physiological megakaryocytic differentiation.

Familial platelet disorder (FPD) is a rare autosomal dominant disorder characterized by thrombocytopenia and abnormal platelet function with its predisposition to acute myelogenous leukemia [18,19]. Patients with this disease harbor monoallelic *RUNX1* mutations. Various types of point mutations, including deletions, missense, nonsense, and frameshift mutations, in *RUNX1* have been identified from more than 20 pedigrees [20–24]. Song *et al.* proposed a model for FPD/AML in which haploinsufficiency of *RUNX1* causes an autosomal dominant congenital platelet defect and predisposes to the acquisition of additional mutations that cause leukemia [25]. Although monoallelic mutations have been implicated in the loss of RUNX1 function as a transcriptional regulator, the details of the molecular events underlying RUNX1-mediated regulation of megakaryocytic gene expression has not yet been clarified.

In view of the situation, in this study, we aimed to elucidate the role of RUNX1 in the regulation of *PF4* expression in megakaryocytic differentiation and to propose a plausible mechanism underlying RUNX1-mediated induction of the FPD phenotype by profiling the functions of 10 different RUNX1 mutants. To this end, we assessed the contribution of RUNX1 to *PF4* expression during megakaryocytic differentiation using an embryonic stem (ES) cell differentiation system. Furthermore, we investigated whether RUNX1 in combination with its interacting factors cooperatively regulates *PF4* expression. Additionally, we analyzed the functional differences between RUNX1 and its mutants with respect to the regulation of *PF4* expression.

Materials and methods

Preparation of plasmids and targeting vectors

The rat PF4 promoter-reporter construct (PF4-luc) and the expression vectors for ETS-1 and FLI-1 (pcDNA3-ETS-1 and pcDNA3-FLI-1, respectively) were previously described [12,26]. To generate expression vectors for RUNX1 and CBFβ, DNA fragments encoding RUNX1 (RUNX1c; a RUNX1 isoform) and CBFβ were amplified by PCR using cDNA from HEL cells and gene-specific primers (Table S1). The resulting PCR fragments were cloned into pcDNA3 vector (Invitrogen, Carlsbad, CA, USA). To generate expression vectors for RUNX1 mutants (Fig. S1), RUNX1 coding sequences in pcDNA3-RUNX1 were mutated by site-directed PCR mutagenesis as previously described [27]. pcDNA3-Flag-RUNX1 was constructed using specific primers coding a Flag tag (Table S1) and pcDNA3-RUNX1 as template in PCR; the product was digested with *Kpn*I and *Sgr*AI and cloned between the *Kpn*I and *Sgr*AI sites of pcDNA3-RUNX1. Expression vectors for Flag-tagged RUNX1 mutants were prepared similarly. The DNA sequences of all constructs were verified by DNA sequencing.

To generate the Hprt-targeting vector containing the PF4 promoter-RUNX1 transgene flanked by 2× core insulators (pMP8III-Core-PF4-RUNX1), a DNA fragment coding RUNX1 was purified from pcDNA3-RUNX1 and cloned into the vector containing the PF4 promoter. The PF4 promoter-RUNX1 fragment was purified generated from the resultant plasmid and cloned into the targeting vector, pMP8III-Core, which was prepared by replacing the *Sal*I site in pMP8II-Core [28] with a *Pme*I site to allow linearization.

Generation and differentiation of ES cells into megakaryocytic cells

ES cells containing the PF4 promoter-RUNX1 transgene flanked with core insulators were prepared according to the previously described method [28]. Established ES cells and control ES cells containing a PF4 promoter-GFP transgene flanked with core insulators were differentiated, as described previously [28]. Briefly, ES cells were differentiated on OP9 stromal cells. The Flk-1$^+$ cells among the differentiated cells were purified by MACS and differentiated into megakaryocytes in a thrombopoietin-containing medium.

Real-time RT-PCR analyses

Total RNA was extracted from differentiated cells using a Nucleospin RNA XS kit (Macherey-Nagel, Düren,

Germany) and 200 ng thereof was reverse transcribed into cDNA with Superscript III reverse transcriptase (Invitrogen). Real-time PCR was performed using gene-specific primers (Table S1), and a QuantiTect SYBR Green PCR Kit (Qiagen, Hilden, Germany). Copy numbers for *RUNX1*, *PF4*, and *GAPDH* were calculated from a plasmid standard curve generated by measuring the known quantity of plasmids containing target sequences.

Cell culture and plasmid transfections

HepG2 and Cos-7 cells were maintained in Dulbecco's modified Eagle's medium supplemented with 10% fetal bovine serum, 100 IU mL^{-1} penicillin, and 100 μg mL^{-1} streptomycin. Cells were seeded and cultured for 24 h before transfection of plasmids using Lipofectamine 2000 (Invitrogen) and then cultured for an additional 48 h.

Reporter gene assays using expression vectors

HepG2 cells (2×10^5) were transfected with 0.5 μg of the reporter plasmid, 0.5 μg of the expression vector, and 0.5 μg of pβactin-lacZ (internal control) and assayed for luciferase and β-galactosidase activity using a Dual-Luciferase Reporter Assay System (Promega, Madison, WI, USA) and AuroraTM Gal-XE chemiluminescent Reporter Gene Assay Kit (MP Biomedicals, Santa Ana, CA, USA), respectively.

Electrophoretic mobility shift assay (EMSA)

In vitro translated RUNX1 was prepared using the TNT Quick Coupled transcription/translation System (Promega) and 1 μg of expression vector. To generate EMSA probes, oligonucleotides (Table S1) were annealed, labeled with T4 polynucleotide kinase and [γ-^{32}P]ATP, and purified with G-50 microcolumns (Amersham Pharmacia Biotech, Uppsala, Sweden). Binding reactions were carried out using 50 fmol of each probe, 2–4 μL of in vitro translated proteins in binding buffer [2 mmol L^{-1} Hepes-NaOH (pH 7.9), 2% glycerol, 0.01 mmol L^{-1} EDTA, 0.25 mmol L^{-1} DTT, 5 mmol L^{-1} KCl, 0.1 mg mL^{-1} bovine serum albumin, 5 ng μL^{-1} poly(dI-dC)] for 40 min at 4 °C. For supershift assays, either anti-RUNX1 antibody (N-20; Santa Cruz Biotechnology, Santa Cruz, CA, USA) or a control antibody was preincubated with the in vitro translated proteins for 10 min before addition of the probe. Samples were electrophoresed in 4% native polyacrylamide gels with 0.5× TBE buffer at 120 V.

Immunocytochemistry

Cos-7 cells (4×10^4) were transfected with 0.3 μg of wild-type or mutant RUNX1 expression vectors and then fixed with 4% paraformaldehyde solution and stained with anti-Flag M2 mouse monoclonal antibody (F1804; Sigma-Aldrich, St. Louis, MO, USA). Alexa Fluor 488–conjugated anti-mouse IgG (Invitrogen) was used as secondary antibody. Cells were then mounted on a slide with Vectashield mounting medium (Vector Laboratories, Burlingame, CA, USA), and fluorescence was detected using a Leica DM2500 microscope equipped with a DFC490 camera (Leica Microsystems, Wetzlar, Germany).

Western blotting using the nuclear and cytoplasmic extracts

Cos-7 cells (5×10^5) were transfected with 2 μg of vector expressing either Flag-tagged RUNX1 or its mutants. Nuclear and cytoplasmic proteins were prepared using a Qproteome Cell Compartment kit (Qiagen) according to the manufacturer's instructions and analyzed by Western blotting using anti-FLAG (M2), anti-LaminB2 (Abcam, Cambridge, UK), and anti-GAPDH (Millipore, Billerica, MA, USA) antibodies.

Immunoprecipitation assay

Cos-7 cells (3×10^6) were transfected with 6 μg of vectors expressing RUNX1, its mutants, CBFβ, ETS-1, or FLI-1. Cell lysates were immunoprecipitated using a FLAG-tagged Protein Immunoprecipitation kit (Sigma-Aldrich). The precipitates were analyzed by western blotting using anti-FLAG (M2), anti-CBFβ (E-20), and anti-ETS-1 (C-20) antibodies (Santa Cruz Biotechnology).

Statistical analyses

The statistical significance of differences between means was determined with Student's *t*-test.

Results

Up-regulated exogenous RUNX1 *expression enhances* PF4 *expression in ES cell–derived megakaryocytes*

To investigate how RUNX1 regulates *PF4* expression during megakaryocytic differentiation, we analyzed the effect of RUNX1 up-regulation on *PF4* expression using our previously established ES cell differentiation system [28], which mimics physiological megakaryocytic differentiation. Two mouse ES cell lines containing the PF4 promoter coupled with *RUNX1* or *GFP* (as a control) in the *Hprt* locus were generated (Fig. 1A) and differentiated into megakaryocytic cells. Real-time RT-PCR analysis confirmed that endogenous mouse *RUNX1* levels were similar in the 2 cell lines, whereas exogenous human *RUNX1* levels were significantly up-regulated in cells harboring the *RUNX1* transgene (Fig. 1B,C). In these cells, the expression of *PF4*, *GPIIb*, and *cMPL* was significantly increased (Fig. 1C, Fig. S1). These data indicate

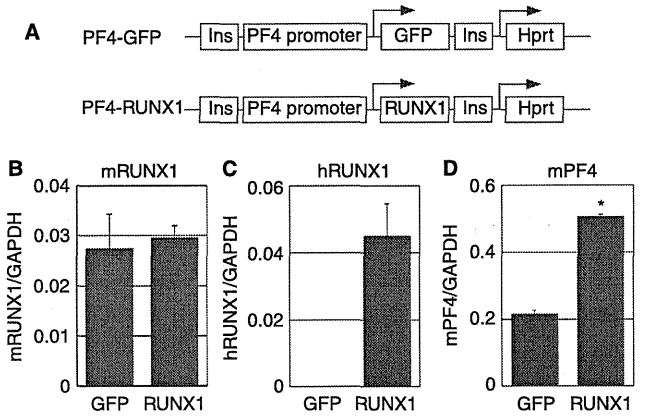

Fig. 1. Exogenous RUNX1 increased *PF4* expression in ES cell-derived megakaryocytes. (A) Two mouse ES cell lines containing a *GFP* (as a control) or human *RUNX1* linked to the *PF4* promoter were prepared. (B, C, and D) Expression of endogenous mRUNX1, exogenous hRUNX1, and PF4 in ES cell-derived megakaryocytes were measured by real-time PCR. Data are represented as the mean ± SE of 3 independent experiments (*$P < 0.05$).

that RUNX1 positively regulates *PF4* expression during megakaryocytic differentiation.

RUNX1 *synergistically activates* PF4 *expression in combination with ETS family proteins*

RUNX1 is known to interact with ETS family proteins ETS-1 and FLI-1, which we have previously identified as transcriptional activators of *PF4* [12,26]. To investigate whether RUNX1 synergistically activates the PF4 promoter in combination with ETS family proteins, cotransfection assays were performed using HepG2 cells. Consistent with the ES cell differentiation system results, up-regulated RUNX1 activated the PF4 promoter (Fig. 2A). Coexpression assays demonstrated that both ETS-1 and FLI-1 in combination with RUNX1 synergistically activated the PF4 promoter (Fig. 2A, B).

To investigate whether the RUNX1-interacting protein CBFβ strengthens the synergistic promoter activation of RUNX1/ETS-1 and RUNX1/FLI-1, coexpression assays were performed. CBFβ expression significantly enhanced PF4 promoter activation by RUNX1/ETS-1 (Fig. 2A). In contrast, CBFβ expression slightly suppressed *PF4* promoter activation by RUNX1/FLI-1 (Fig. 2B). Thus, CBFβ expression is essential for maximum *PF4* promoter activation by RUNX1/ETS-1 but not by RUNX1/FLI-1.

RUNX1 *mutants fail to activate the PF4 promoter in the presence of either ETS-1 or FLI-1*

To investigate whether FPD RUNX1 mutants synergistically activate the PF4 promoter, coexpression assays were performed with expression vectors for various types of RUNX1 mutants (Figs. 3A and S2). Interestingly, all RUNX1 mutants failed to activate the PF4 promoter in the presence of ETS-1 and CBFβ (Fig. 3B). Unlike the RUNX1 mutant Y287X, which showed only impaired synergistic activation, the other RUNX1 mutants failed to activate the PF4 promoter in the presence of FLI-1 (Fig. 3C). Collectively, these results demonstrated that all FPD RUNX1 mutants partially or completely lost the ability to synergistically activate the PF4 promoter in the presence of ETS-1, CBFβ, and FLI-1.

DNA-binding activity of RUNX1 mutants

To elucidate the reason for the inability of RUNX1 mutants to activate the PF4 promoter in the presence of its interacting proteins, the DNA-binding activity of RUNX1 mutants was evaluated by EMSA, using a probe spanning the RUNX1 consensus binding motif and recombinant proteins (Fig. 4A). Shifted bands were observed in the lanes corresponding to wild-type RUNX1 and the A134P, R166Q, Y287X, and T246fs (T246Rfs*8) but not other mutants. All the shifted bands were supershifted on addition of anti-RUNX1 antibody but not control antibody. These data indicated that the RUNX1 mutants K110E, D198Y, R201Q, R204X, R201X, and F163fs (F163Efs*43) completely lost DNA-binding activity.

Subcellular localization of RUNX1 mutants

EMSA analyses revealed that loss of DNA-binding activity is responsible for insufficient promoter activation by several RUNX1 mutants; however, it was unclear why the other mutants failed to activate the PF4 promoter. To investigate this, cellular localization of Flag-tagged wild-type and mutant RUNX1 were analyzed by immunocytochemistry and by Western blotting of nuclear and cytoplasmic extracts using Cos-7 cells (Fig. 5). In both experiments, wild-type RUNX1 was observed predominantly in the nucleus. K110E, A134P, R166Q, D198Y, and R201Q mutants were observed both in the nucleus and in the cytoplasm; the ratio between nuclear and

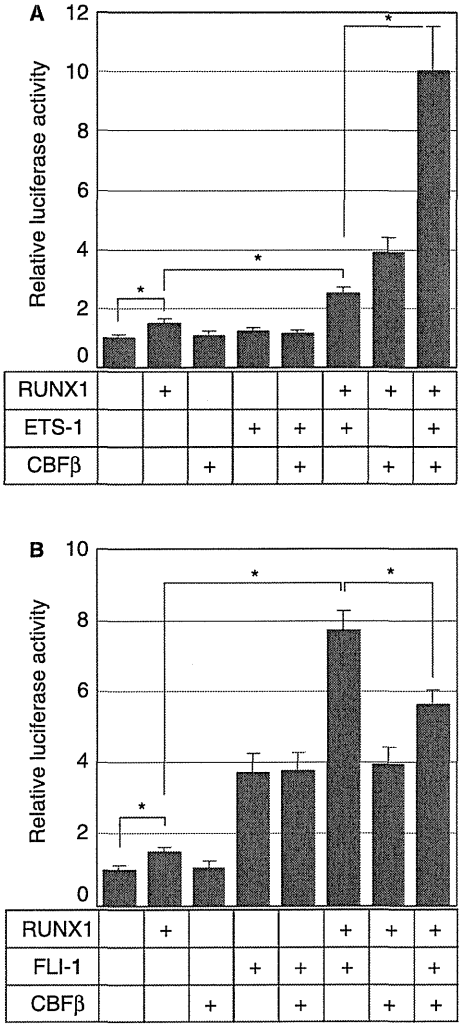

Fig. 2. RUNX1 synergistically activated the *PF4* promoter with ETS-1, CBFβ, and FLI-1. (A) Coexpression assays were performed with HepG2 cells using the PF4 promoter-luciferase reporter plasmid and expression vectors for RUNX1, ETS-1, and CBFβ. (B) Coexpression assays were performed with HepG2 cells using the PF4 promoter-luciferase reporter plasmid and expression vectors for RUNX1, FLI-1, and CBFβ. Data in A and B are represented as the mean ± SE of 3 independent experiments (*$P < 0.05$).

cytoplasmic localization varied among these mutants. The other mutants were detected predominantly in the cytoplasm. Together, these results suggested that RUNX1 mutants harboring a single amino acid substitution tend to localize both in the nucleus and the cytoplasm, whereas those that lack the C-terminal region localize predominantly in the cytoplasm.

Interaction of RUNX1 mutants with ETS-1, FLI-1, and CBFβ

The interaction of RUNX1 mutants with ETS-1, FLI-1, and CBFβ was investigated using immunoprecipitation assays. R166Q and F163fs mutants demonstrated a strong binding affinity for ETS-1, the D198Y mutant showed a moderately strong affinity, whereas Y287 and R201X mutants had a weak affinity (Fig. 6A). However, there was no significant change in the binding affinities of ETS-1 for the other mutants. In contrast, only the R201X mutant had a strong binding affinity for CBFβ, while the K110E, A134P, R166Q, D198Y, R201Q, Y287X, and F163fs mutants showed a weak affinity (Fig. 6B). No significant change was observed in the affinities of CBFβ in presence of T246fs and R204X mutants. While the binding affinities of R166Q, D198Y, R201Q, Y287X, T246fs, and F163fs mutants for FLI-1 were strong, the K110E mutant showed a weak affinity (Fig. 6C). There was no significant change in the affinities of A134P, R204X, and R201X mutants for FLI-1. These results indicated that the affinity of each RUNX1 mutant for ETS-1, CBFβ, or FLI-1 is specific and that the influence of each mutant on these interaction varies.

Discussion

The present study demonstrated that RUNX1, but not its mutants, synergistically activates *PF4* expression in combination with CBFβ, ETS-1, and FLI-1 during megakaryocytic differentiation. Additionally, our study highlighted that monoallelic RUNX1 mutants found in FPD patients cause various functional defects, including loss of DNA-binding activity, abnormal subcellular localization, and/or changes in binding affinities for ETS-1, CBFβ, and FLI-1, thus leading to pathogenicity.

We had previously reported that RUNX1 suppresses the expression of megakaryocyte-specific genes in TPO-treated UT-7/GM cells. Additionally, our unpublished data indicate that RUNX1 down- and up-regulates *PF4* expression in megakaryocytic and nonmegakaryocytic cells, respectively. We speculated that these cell type–specific results, which was previously addressed by Pendaries *et al.* [29], are partially due to cell type–specific interacting proteins. To overcome this, we had recently established an ES cell differentiation system in which exogenous RUNX1 could be overexpressed in a megakaryocytic lineage-specific manner during megakaryocytic differentiation [28]. Using this system, we successfully demonstrated that RUNX1 up-regulates *PF4* expression during megakaryocytic differentiation. However, it is technically impossible to perform assays such as reporter gene assays and protein extraction with this system, because of the limited number of differentiated cells. Therefore, we opted to use nonmegakaryocytic cells (HepG2 and Cos-7 cells), which are used for functional analysis of megakaryocytic transcription factors [12,14,15,22] and in which RUNX1 functions as a positive regulator of *PF4* expression.

However, expression of RUNX1 alone does not result in strong activation of the PF4 promoter in transiently transfected HepG2 cells. This led us to speculate that RUNX1 possibly interacts with other factors, thereby strongly activating the PF4 promoter. Indeed, ETS-1 and

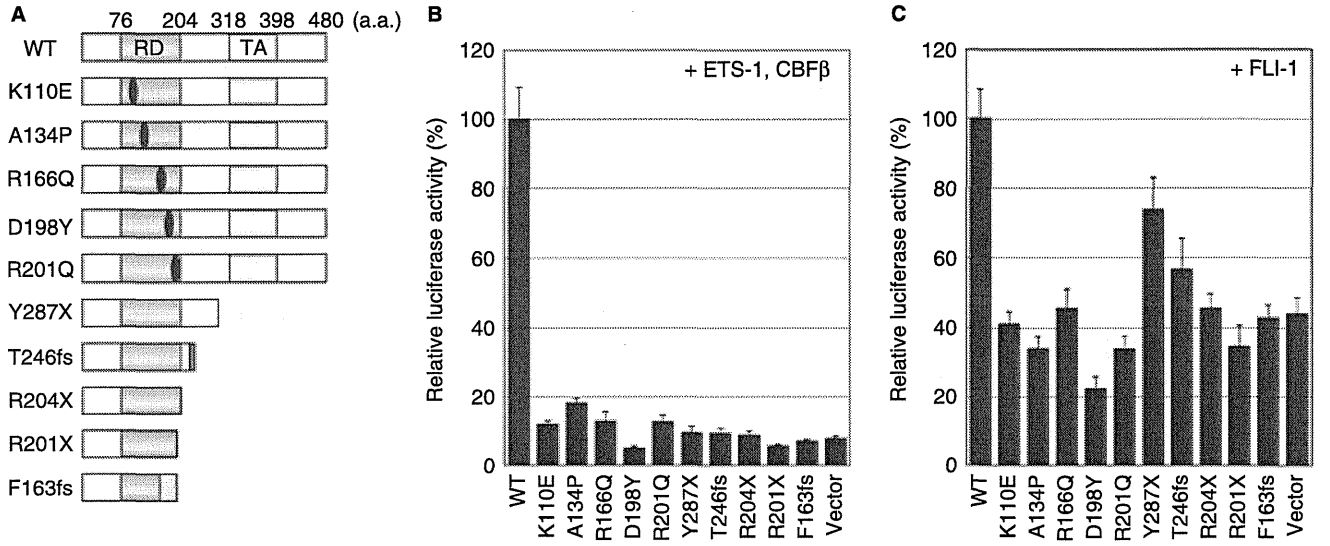

Fig. 3. Ability of 10 familial platelet disorder (FPD)-causing RUNX1 mutants to mediate *PF4* promoter activation. (A) Wild-type RUNX1 and 10 RUNX1 mutants found in FPD. RD and TA indicate the runt domain and transactivation domain, respectively. (B) Coexpression assays were performed with HepG2 cells using the PF4 promoter-luciferase reporter plasmid and expression vectors for wild-type or mutant RUNX1, ETS-1, and CBFβ. (C) Coexpression assays were performed with HepG2 cells using the PF4 promoter-luciferase reporter plasmid and expression vectors for wild-type or mutant RUNX1, and FLI-1. Data in B and C are represented as the mean ± SE of at least 3 independent experiments.

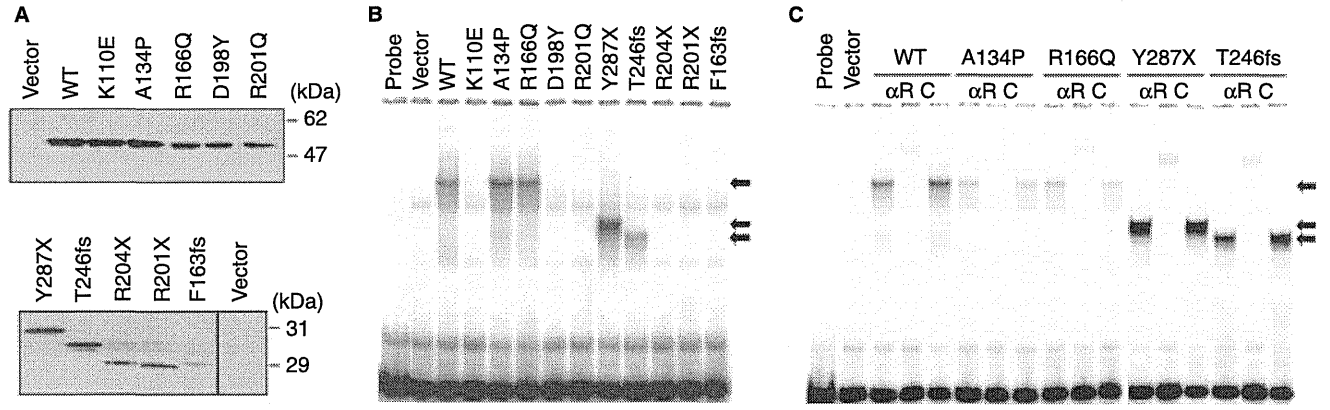

Fig. 4. DNA-binding activity of RUNX1 mutants. (A) Recombinant RUNX1 and RUNX1 mutants were prepared using an *in vitro* transcription/translation system using expression vectors for RUNX1 or an empty vector (Vector). Protein production was confirmed by western blotting. (B) EMSA was performed with the recombinant RUNX1 proteins and a probe containing the consensus RUNX1-binding motif. Arrows indicate the specific shifted bands. (C) Supershift assays were performed with recombinant RUNX1 and RUNX1 mutants, a RUNX1 antibody, and control IgG. Arrows indicate shifted bands observed in B. Representative results from at least 3 independent experiments are shown in A, B, and C.

FLI-1, which we had previously identified as activators of *PF4* expression, synergistically activate the PF4 promoter in combination with RUNX1. Interestingly, CBFβ expression enhanced PF4 promoter activation in the presence of RUNX1/ETS-1, but not of RUNX1/FLI-1. This implies that RUNX1 may function as 2 distinct protein complexes, RUNX1/CBFβ/ETS-1 and RUNX1/FLI-1, in megakaryocytes. The roles played by these 2 complexes in the regulation of *PF4* expression remains to be elucidated.

Our previous study showed that ETS-1 expression levels gradually decrease, while those of FLI-1 gradually increase, during megakaryocytic differentiation [12]. Additionally, differentiation stage–specific interaction between RUNX1 and FLI-1 and a functional switch of RUNX1 have been reported [10,11]. Taken together, these findings suggest that RUNX1 is a pivotal factor for the formation of differentiation stage-specific functional transcription factor complexes and that RUNX1/CBFβ/ETS-1 functions early, while RUNX1/FLI-1 acts later in megakaryo-

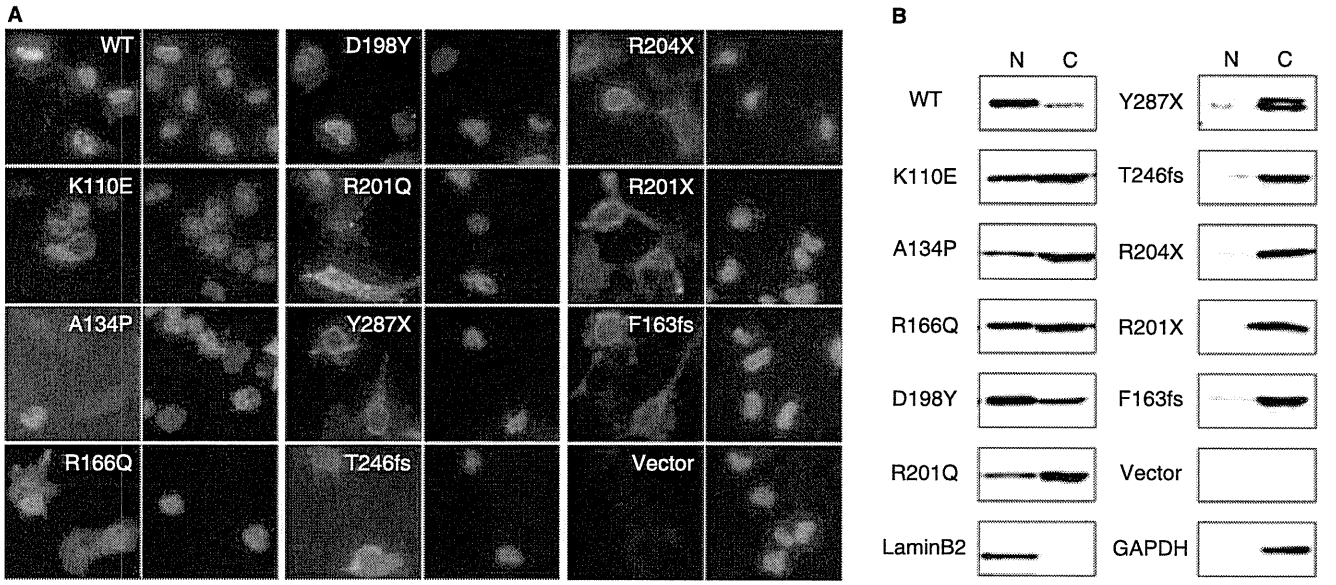

Fig. 5. Subcellular localization of RUNX1 mutants. Flag-tagged RUNX1 and RUNX1 mutants were expressed in Cos-7 cells. (A) Immunocytochemistry was performed with anti-Flag antibody and DAPI. (B) Nuclear and cytoplasmic protein fractions prepared from transfected Cos-7 cells were analyzed by Western blotting using anti-Flag, anti-LaminB1 (nuclear protein), and anti-GAPDH (cytoplasmic protein) antibodies. Representative results from 3 independent experiments are shown in A and B.

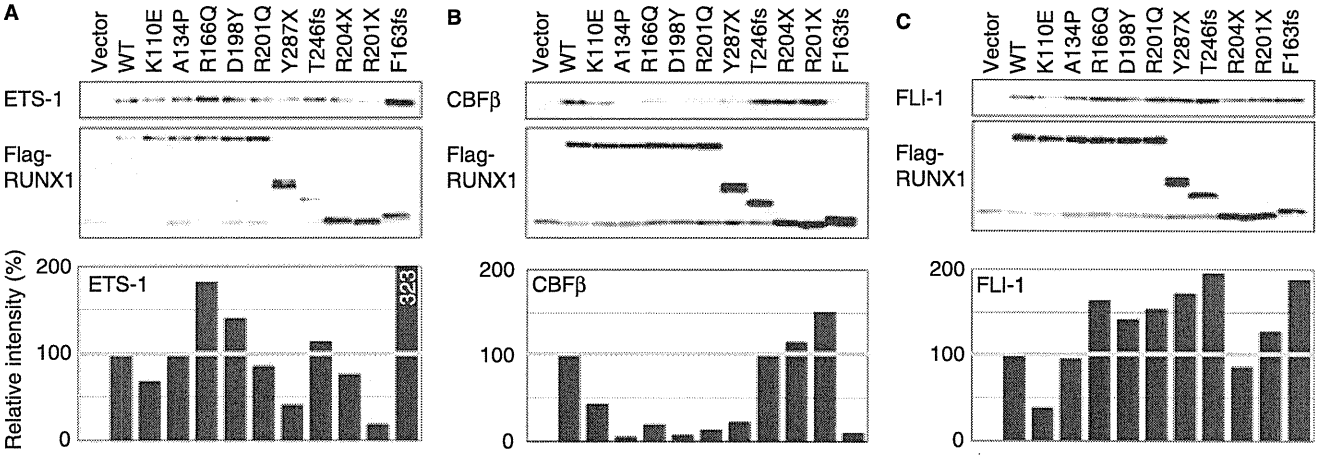

Fig. 6. Interaction of RUNX1 mutants with ETS-1, CBFβ, and FLI-1. Immunoprecipitation was performed with anti-Flag antibody and protein mixtures containing Flag-tagged RUNX1 and either ETS-1, CBFβ, or FLI-1. The precipitated proteins were analyzed by western blotting. Representative results from at least 3 independent experiments are shown in A, B, and C.

cytic differentiation. In addition, we speculate that the RUNX1/FLI-1 complex includes other components, because no strong synergism is observed between RUNX1 and FLI-1 compared with that between RUNX1 and ETS-1 (Fig. 2) and because FLI-1 does not synergistically activate the promoter with CBFβ. Previously, we demonstrated that GATA-1 strongly and synergistically activates the PF4 promoter with FLI-1 but not with the other ETS family proteins, including ETS-1 [12,13]. This suggests the possibility that the RUNX1/FLI-1/GATA-1 complex is formed in megakaryocytes and contributes to the strong promoter activation, but this requires further study.

Although an earlier study reported that RUNX mutants have reduced DNA binding activity and fail to activate the M-CSF promoter [22], a detailed mechanism underlying the regulation of megakaryocytic gene expression by RUNX1 mutants has not yet been clarified. Our findings here demonstrated that RUNX1 mutants are not capable of strongly activating *PF4* expression by interacting with either ETS-1 or FLI-1. This implies that loss of RUNX1 function as a transcriptional activator leads to an aberrant megakaryocytic gene expression, which in turn hinders normal platelet production and function, thus inducing the FPD phenotype.

Table 1 Summary of the functional analyzes of wild-type RUNX1 and the mutants

				Interaction		
	Promoter activation	DNA binding	Localization	ETS-1	CBFβ	FLI-1
WT	+	+	N/c	1	1	1
K110E	–	–	N/C	0.7	0.4	0.4
A134P	–	+	N/C	1	0.1	1
R166Q	–	+	N/C	1.8	0.2	1.6
D198Y	–	–	N/C	1.4	0.1	1.4
R201Q	–	–	N/C	0.8	0.1	1.5
Y287X	–	+	n/C	0.4	0.2	1.7
T246fs	–	+	n/C	1.1	1	2
R204X	–	–	n/C	0.8	1.1	0.9
R201X	–	–	n/C	0.2	1.5	1.3
F163fs	–	–	n/C	3.2	0.1	1.9

Furthermore, the findings of our study revealed that partial/incomplete PF4 promoter activation is induced by 3 different mechanisms, which, in turn, depend on various functional abnormalities caused by RUNX1 mutations (Table 1). First, among the 10 RUNX1 mutants studied, 6 of them had completely lost DNA-binding activity. Unexpectedly, the mutants A134P and R166Q, which exhibited mutations in the runt domain, retained DNA-binding activity, thus suggesting that mutations in the runt domain do not necessarily cause loss of DNA-binding activity. All RUNX1 mutants showed abnormal cytoplasmic localization. Full-length RUNX1 mutants were detected in both the nucleus and cytoplasm, whereas truncated RUNX1 mutants mostly failed to localize to the nucleus, suggesting that the C-terminal region is crucial for nuclear localization. Moreover, the binding affinities of RUNX1 mutants for ETS-1, CBFβ, and FLI-1 were altered. Notably, most of the RUNX1 mutants exhibited strong binding affinity for ETS-1 and FLI-1 but weak binding affinities for CBFβ. This suggested the possibility that both weak and strong interactions of these mutants with other factors may hamper maximum PF4 promoter activation, and thus RUNX1 mutants fail to function as transcriptional activators.

In conclusion, the present study highlights the functional effects of monoallelic RUNX1 mutations helping to elucidate the pathoetiology of FPD. Future studies investigating each RUNX1 mutant in detail are warranted to understand the correlation between a specific RUNX1 mutation type and FPD phenotype that may allow development of targeted therapies.

Addendum

Experimental design: Y. Okada, M. Watanabe, T. Nakai, Y. Kamikawa, M. Shimizu, M. Yonekura, E. Matsuura, Y. Fukuhara, Y. Hoshika, R. Nagai, W.C. Aird, and T. Doi. Performed experiments: Y. Okada, M. Watanabe, T. Nakai, Y. Kamikawa, M. Shimizu, M. Yonekura, E. Matsuura, Y. Fukuhara, Y. Hoshika, and R. Nagai. Data analysis: Y. Okada, M. Watanabe, T. Nakai, Y. Kamikawa, M. Shimizu, M. Yonekura, E. Matsuura, Y. Fukuhara, Y. Hoshika, R. Nagai, W.C. Aird, and T. Doi. Manuscript drafting: Y. Okada, M. Watanabe, and T. Doi.

Acknowledgements

We thank Mie Kitayama, Hironori Nagura, Emi Nakata, Atsuko Wakimura, Dr. Noubuaki Funahashi, Dr. Nobumasa Hino, and Dr. Kenji Ishimoto for technical support and helpful suggestions. We also thank Dr. Sarah Bronson and Dr. Kenji Kitajima for the gift of BK4 and OP9 cells, respectively. TPO was kindly provided by Kyowa Hakko Kirin. This work was supported by JSPS KAKENHI, MEXT KAKENHI, the Takeda Science Foundation, and the Mitsubishi Pharma Research Foundation, Japan.

Disclosure of Conflicts of Interest

The authors state that they have no conflict of interest.

Supporting Information

Additional Supporting Information may be found in the online version of this article:

Figure S1. Exogenous RUNX1 increased megakaryocyte-specific gene expression in ES cell-derived megakaryocytes.
Figure S2. Wild type RUNX1c and sites of mutation.
Table S1. Oligonucleotide sequences for primers and a probe.

References

1 Okuda T, van Deursen J, Hiebert SW, Grosveld G, Downing JR. AML1, the target of multiple chromosomal translocations in human leukemia, is essential for normal fetal liver hematopoiesis. *Cell* 1996; **84**: 321–30.

2 Wang Q, Stacy T, Binder M, Marin-Padilla M, Sharpe AH, Speck NA. Disruption of the Cbfa2 gene causes necrosis and hemorrhaging in the central nervous system and blocks definitive hematopoiesis. *Proc Natl Acad Sci USA* 1996; **93**: 3444–9.

3 Ichikawa M, Asai T, Saito T, Seo S, Yamazaki I, Yamagata T, Mitani K, Chiba S, Ogawa S, Kurokawa M, Hirai H. AML-1 is required for megakaryocytic maturation and lymphocytic differentiation, but not for maintenance of hematopoietic stem cells in adult hematopoiesis. *Nat Med* 2004; **10**: 299–304.

4 Sasaki K, Yagi H, Bronson RT, Tominaga K, Matsunashi T, Deguchi K, Tani Y, Kishimoto T, Komori T. Absence of fetal liver hematopoiesis in mice deficient in transcriptional coactivator core binding factor beta. *Proc Natl Acad Sci USA* 1996; **93**: 12359–63.

5 Niki M, Okada H, Takano H, Kuno J, Tani K, Hibino H, Asano S, Ito Y, Satake M, Noda T. Hematopoiesis in the fetal liver is impaired by targeted mutagenesis of a gene encoding a non-DNA binding subunit of the transcription factor, polyomavirus enhancer binding protein 2/core binding factor. *Proc Natl Acad Sci USA* 1997; **94**: 5697–702.

6 Wang Q, Stacy T, Miller JD, Lewis AF, Gu TL, Huang X, Bushweller JH, Bories JC, Alt FW, Ryan G, Liu PP, Wynshaw-Boris A, Binder M, Marin-Padilla M, Sharpe AH, Speck NA. The CBFbeta subunit is essential for CBFalpha2 (AML1) function in vivo. *Cell* 1996; **87**: 697–708.

7 Elagib KE, Racke FK, Mogass M, Khetawat R, Delehanty LL, Goldfarb AN. RUNX1 and GATA-1 coexpression and cooperation in megakaryocytic differentiation. *Blood* 2003; **101**: 4333–41.

8 Lutterbach B, Westendorf JJ, Linggi B, Isaac S, Seto E, Hiebert SW. A mechanism of repression by acute myeloid leukemia-1, the target of multiple chromosomal translocations in acute leukemia. *J Biol Chem* 2000; **275**: 651–6.

9 Kim WY, Sieweke M, Ogawa E, Wee HJ, Englmeier U, Graf T, Ito Y. Mutual activation of Ets-1 and AML1 DNA binding by direct interaction of their autoinhibitory domains. *EMBO J* 1999; **18**: 1609–20.

10 Huang H, Yu M, Akie TE, Moran TB, Woo AJ, Tu N, Waldon Z, Lin YY, Steen H, Cantor AB. Differentiation-dependent interactions between RUNX-1 and FLI-1 during megakaryocyte development. *Mol Cell Biol* 2009; **29**: 4103–15.

11 Satoh Y, Matsumura I, Tanaka H, Ezoe S, Fukushima K, Tokunaga M, Yasumi M, Shibayama H, Mizuki M, Era T, Okuda T, Kanakura Y. AML1/RUNX1 works as a negative regulator of c-Mpl in hematopoietic stem cells. *J Biol Chem* 2008; **283**: 30045–56.

12 Okada Y, Nobori H, Shimizu M, Watanabe M, Yonekura M, Nakai T, Kamikawa Y, Wakimura A, Funahashi N, Naruse H, Watanabe A, Yamasaki D, Fukada S, Yasui K, Matsumoto K, Sato T, Kitajima K, Nakano T, Aird WC, Doi T. Multiple ETS family proteins regulate PF4 gene expression by binding to the same ETS binding site. *PLoS ONE* 2011; **6**: e24837.

13 Okada Y, Nagai R, Sato T, Matsuura E, Minami T, Morita I, Doi T. Homeodomain proteins MEIS1 and PBXs regulate the lineage-specific transcription of the platelet factor 4 gene. *Blood* 2003; **101**: 4748–56.

14 Okada Y, Matsuura E, Tozuka Z, Nagai R, Watanabe A, Matsumoto K, Yasui K, Jackman RW, Nakano T, Doi T. Upstream stimulatory factors stimulate transcription through E-box motifs in the PF4 gene in megakaryocytes. *Blood* 2004; **104**: 2027–34.

15 Okada Y, Matsuura E, Nagai R, Sato T, Watanabe A, Morita I, Doi T. PREP1, MEIS1 homolog protein, regulates PF4 gene expression. *Biochem Biophys Res Commun* 2003; **305**: 155–9.

16 Nagai R, Matsuura E, Hoshika Y, Nakata E, Nagura H, Watanabe A, Komatsu N, Okada Y, Doi T. RUNX1 suppression induces megakaryocytic differentiation of UT-7/GM cells. *Biochem Biophys Res Commun* 2006; **345**: 78–84.

17 Aneja K, Jalagadugula G, Mao G, Singh A, Rao AK. Mechanism of platelet factor 4 (PF4) deficiency with RUNX1 haplodeficiency: RUNX1 is a transcriptional regulator of PF4. *J Thromb Haemost* 2011; **9**: 383–91.

18 Dowton SB, Beardsley D, Jamison D, Blattner S, Li FP. Studies of a familial platelet disorder. *Blood* 1985; **65**: 557–63.

19 Ho CY, Otterud B, Legare RD, Varvil T, Saxena R, DeHart DB, Kohler SE, Aster JC, Dowton SB, Li FP, Leppert M, Gilliland DG. Linkage of a familial platelet disorder with a propensity to develop myeloid malignancies to human chromosome 21q22.1-22.2. *Blood* 1996; **87**: 5218–24.

20 Preudhomme C, Renneville A, Bourdon V, Philippe N, Roche-Lestienne C, Boissel N, Dhedin N, Andre JM, Cornillet-Lefebvre P, Baruchel A, Mozziconacci MJ, Sobol H. High frequency of RUNX1 biallelic alteration in acute myeloid leukemia secondary to familial platelet disorder. *Blood* 2009; **113**: 5583–7.

21 Owen CJ, Toze CL, Koochin A, Forrest DL, Smith CA, Stevens JM, Jackson SC, Poon MC, Sinclair GD, Leber B, Johnson PR, Macheta A, Yin JA, Barnett MJ, Lister TA, Fitzgibbon J. Five new pedigrees with inherited RUNX1 mutations causing familial platelet disorder with propensity to myeloid malignancy. *Blood* 2008; **112**: 4639–45.

22 Michaud J, Wu F, Osato M, Cottles GM, Yanagida M, Asou N, Shigesada K, Ito Y, Benson KF, Raskind WH, Rossier C, Antonarakis SE, Israels S, McNicol A, Weiss H, Horwitz M, Scott HS. In vitro analyses of known and novel RUNX1/AML1 mutations in dominant familial platelet disorder with predisposition to acute myelogenous leukemia: implications for mechanisms of pathogenesis. *Blood* 2002; **99**: 1364–72.

23 Kirito K, Sakoe K, Shinoda D, Takiyama Y, Kaushansky K, Komatsu N. A novel RUNX1 mutation in familial platelet disorder with propensity to develop myeloid malignancies. *Haematologica* 2008; **93**: 155–6.

24 Buijs A, Poddighe P, van Wijk R, van Solinge W, Borst E, Verdonck L, Hagenbeek A, Pearson P, Lokhorst H. A novel CBFA2 single-nucleotide mutation in familial platelet disorder with propensity to develop myeloid malignancies. *Blood* 2001; **98**: 2856–8.

25 Song WJ, Sullivan MG, Legare RD, Hutchings S, Tan X, Kufrin D, Ratajczak J, Resende IC, Haworth C, Hock R, Loh M, Felix C, Roy DC, Busque L, Kurnit D, Willman C, Gewirtz AM, Speck NA, Bushweller JH, Li FP, *et al.* Haploinsufficiency of CBFA2 causes familial thrombocytopenia with propensity to develop acute myelogenous leukaemia. *Nat Genet* 1999; **23**: 166–75.

26 Minami T, Tachibana K, Imanishi T, Doi T. Both Ets-1 and GATA-1 are essential for positive regulation of platelet factor 4 gene expression. *Eur J Biochem* 1998; **258**: 879–89.

27 Okada Y, Yano K, Jin E, Funahashi N, Kitayama M, Doi T, Spokes K, Beeler DL, Shih SC, Okada H, Danilov TA, Maynard E, Minami T, Oettgen P, Aird WC. A three-kilobase fragment of the human Robo4 promoter directs cell type-specific expression in endothelium. *Circ Res* 2007; **100**: 1712–22.

28 Okada Y, Yonekura M, Watanabe M, Nakai T, Wakimura A, Shimizu M, Kamikawa Y, Kitayama M, Kitajima K, Aird WC, Doi T. Embryonic stem cell differentiation system for evaluating gene functions involved in physiological megakaryocytic differentiation. *Biochem Biophys Res Commun* 2012; **149**: 477–81.

29 Pendaries C, Watson SP, Spalton JC. Methods for genetic modification of megakaryocytes and platelets. *Platelets* 2007; **18**: 393–408.

J. Biochem. 2013;154(3):265–273 doi:10.1093/jb/mvt050

JB THE JOURNAL OF BIOCHEMISTRY

Human mannose-binding lectin 2 is directly regulated by peroxisome proliferator-activated receptors via a peroxisome proliferator responsive element

Received March 18, 2013; accepted May 16, 2013; published online May 27, 2013

Keisuke Tachibana[1,*], Kentaro Takeuchi[1,*], Hirohiko Inada[1,*], Ken Sugimoto[2], Kenji Ishimoto[1,2], Masanori Yamashita[1], Takashi Maegawa[1], Daisuke Yamasaki[1,3], Shigehiro Osada[4], Toshiya Tanaka[5], Hiromi Rakugi[2], Takao Hamakubo[5,6], Juro Sakai[5], Tatsuhiko Kodama[5] and Takefumi Doi[1,2,3,†]

[1]Graduate School of Pharmaceutical Sciences, Osaka University, 1-6 Yamadaoka, Suita, Osaka 565-0871, Japan; [2]Graduate School of Medicine, Osaka University, 2-2 Yamadaoka, Suita, Osaka 565-0871, Japan; [3]The Center for Advanced Medical Engineering and Informatics, Osaka University, 2-2 Yamadaoka, Suita, Osaka 565-0871, Japan; [4]Graduate School of Pharmaceutical Sciences, Nagoya City University, 3-1 Tanabe-dori, Mizuho-ku, Nagoya, Aichi 467-8603, Japan; [5]Laboratory for System Biology and Medicine, Research Center for Advanced Science and Technology, University of Tokyo, 4-6-1 Komaba, Meguro, Tokyo 153-8904, Japan; and [6]Department of Quantitative Biology and Medicine, Research Center for Advanced Science and Technology, University of Tokyo, 4-6-1 Komaba, Meguro, Tokyo 153-8904, Japan

*These authors contributed equally to this work.

†Takefumi Doi, Graduate School of Pharmaceutical Sciences, Osaka University, 1-6 Yamadaoka, Suita, Osaka 565-0871, Japan. Tel/Fax: +81-6-6879-8158, email: doi@phs.osaka-u.ac.jp

Human mannose-binding lectin (MBL) is encoded by the MBL2 gene and is a key player in innate immunity. However, the mechanism of the transcriptional regulation of MBL2 is largely unknown. The peroxisome proliferator-activated receptors (PPARs) are ligand-activated transcription factors that play an important role in a number of biological responses, including lipid homeostasis, immune function and adipogenesis. In this study, we showed that PPARα and PPARγ up-regulate the expression of human MBL2. Using a luciferase assay, electrophoretic mobility-shift assay and chromatin immunoprecipitation assay, we demonstrated that PPARs regulate the expression of human MBL2 via the peroxisome proliferator responsive element (PPRE). On the other hand, MBL2 mRNA expression was not affected by the PPARα ligand both *in vivo* in rat liver and *in vitro* in rat H4IIE hepatoma cells. Thus, there is a species difference in regulation of MBL2 gene expression by PPARs between humans and rodents. We also show that the species differences in response to PPAR could be due in part to sequence-specific differences in the PPRE in the promoter region of MBL2. These results indicate that human, but not rat, MBL2 expression is regulated by PPARs via a PPRE.

Keywords: MBL2/PPAR alpha/PPAR gamma/PPRE/species difference.

Abbreviations: ACO, acyl-CoA oxidase; DR1, direct repeat of two hexanucleotides, spaced by one nucleotide; MBL, mannose-binding lectin; PPAR, peroxisome proliferator-activated receptor; PPRE, peroxisome proliferator responsive element; RXR, retinoid X receptor.

The mannose-binding lectin 2 (MBL2) gene encodes a plasma protein MBL that is secreted by the liver. MBL is a member of the collectin family and is important in innate immunity (*1*). Interestingly, in humans, MBL deficiency has been correlated with severity of atherosclerotic disease (*2*). Moreover, MBL is present in early atherosclerotic regions, and has anti-atherosclerotic effects by facilitating macrophage clearance of modified forms of low-density lipoprotein (*3*, *4*). Therefore, drugs increasing the amount of MBL are attractive candidates for anti-atherogenic therapy. However, little is known about transcription factors that regulate human MBL2 promoter activity (*5*).

The peroxisome proliferator-activated receptors (PPARs) are ligand-activated transcription factors that belong to the nuclear hormone receptor superfamily. PPARs bind to a direct repeat of two hexanucleotides, spaced by one nucleotide (DR1 motif) as heterodimers with the retinoid X receptor (RXR) (*6*). PPARα plays a central role in the control of fatty acid oxidation, lipid and lipoprotein metabolism, and inflammatory responses in liver. PPARα activators have been used to treat dyslipidemia, causing a reduction in plasma triglyceride and elevation of high-density lipoprotein (HDL) cholesterol (*7*). PPARγ has two isoforms: PPARγ1 and PPARγ2. PPARγ1 is expressed in the liver, the immune system (*e.g.*, monocytes and macrophages) and in other tissues. On the other hand, PPARγ2 is exclusively expressed in adipose tissue and represents a potential therapeutic target of type 2 diabetes (*8*). Moreover, clinical studies suggested that PPARs are good therapeutic targets for atherosclerosis (*9*).

In this study we investigated the relationship between PPARs and MBL2, to elucidate the molecular mechanism underlying the anti-atherogenic effect of PPARs. We showed that human MBL2 is positively regulated by both PPARα and PPARγ in human hepatoma cells. To gain new insights into the transcriptional regulation of human MBL2, we analysed the promoter region of MBL2. We showed that PPARα

Table I. Primers used for real-time PCR analysis.

Gene		Sequence	Size (bp)
Human MBL2	For. primer :	AGTCCGGATGGTGATAGTAGCC	107
	Rev. primer :	CCAACTTGTTTGCCCAGAGA	
Human Cyclophilin A	For. primer :	GCGTCTCCTTTGAGCTGTTT	142
	Rev. primer :	TCACCACCCTGACACATAAACC	
Rat MBL2	For. primer :	CCTGGGTCAAAAGGAGCAAC	202
	Rev. primer :	TCGCTCTGTTAAGGGGCATC	
Rat ACO	For. primer :	TTCGAGGCTTGGAAACCACT	204
	Rev. primer :	GGGTCCCAATTTCACGGATA	
Rat β2-microglobulin	For. primer :	GCTCGGTGACCGTGATCTTT	156
	Rev. primer :	TCTGAGGTGGGTGGAACTGA	

Sequences of forward (For.) and reverse (Rev.) primer for each target are shown. Sequences are 5′–3′.

and PPARγ regulate the expression of human MBL2 via the peroxisome proliferator responsive element (PPRE). In contrast, the PPARα ligand did not result in any changes in MBL2 mRNA expression both *in vivo* in rat liver and *in vitro* in rat hepatoma cells. We also show that the species differences in response to PPAR could be due in part to sequence-specific differences in the PPRE in the promoter region of MBL2. These results indicate that human, but not rat, MBL2 expression is regulated by PPARs via a PPRE. This novel finding that human MBL2 expression is regulated by PPAR suggests a potential therapeutic effect of PPAR ligands in the treatment of atherosclerosis.

Materials and Methods

Plasmid construction

A human MBL2 promoter fragment spanning −4942 bp to +68 bp was obtained by means of PCR with a HepG2 genome and cloned into PGV-B vector (Toyo Ink, Tokyo, Japan) to generate a reporter plasmid (hMBL2-Luc). Deletion constructs were generated by digestion of hMBL2-Luc. A mutant reporter plasmid, hMBL2-Luc (mut), was constructed by introducing point mutations into the human MBL2 promoter using PCR methods. Both hMBL2-PPRE and rMBL2-DR1 plasmids were obtained by ligating the corresponding double-stranded oligonucleotides (5′-CAGATTGTAGGACAGAG GGCATGCTCGG-3′ for hMBL2-PPRE and 5′-CAAGTTACAG GACAGAGGCAGGGTTGGT-3′ for rMBL2-DR1) to a PGV-P2 vector (Toyo Ink). All constructs were verified by sequencing.

Cell culture and ligand treatments

HepG2 human hepatoblastoma cells and Huh-7 human hepatoma cells were cultured in Dulbecco's Modified Eagle's Medium (DMEM) (Nacalai tesque, Kyoto, Japan) containing 7.5% fetal bovine serum (FBS) (Biowest, Nuaillé, France), 100 IU/ml penicillin and 100 μg/ml streptomycin (Nacalai tesque). The tightly tetracycline (Tet)-regulatable HepG2-tet-off-hPPARα and hPPARγ1 cells (*10*) were cultured in DMEM containing 10% FBS, 2 μg/ml Tet (Wako Pure Chemicals, Osaka, Japan), 100 IU/ml penicillin and 100 μg/ml streptomycin. H4IIE rat hepatoma cells were cultured in α-MEM (Nacalai tesque) containing 10% FBS, 100 IU/ml penicillin and 100 μg/ml streptomycin. For ligand treatment, cells were cultured in DMEM supplemented with 10% HyClone Charcoal/Dextran Treated FBS (Thermo Scientific, Rockford, IL) and either GW7647 (Sigma-Aldrich, St. Louis, MO), rosiglitazone (Alexis Biochemicals, Farmingdale, NY) or DMSO.

Animal treatments

Male Fischer F344 rats, purchased from Charles River Japan Inc. (Yokohama, Japan), were maintained in the animal facilities of Osaka University Medical School in an air-conditioned room (22–25°C) with a 12 h light/dark cycle and were given free access to food (standard chow) and water. Rats at 13 weeks of age, fenofibrate (Sigma-Aldrich) was suspended in 0.5% methylcellulose (400 cP, Wako Pure Chemicals) and was administered by gavage at 400 mg/kg body weight per day for 4 days. All rats were killed under anesthesia by intraperitoneal administration of pentobarbital (0.3 mg/g body weight) and liver was isolated. All experiments were performed according to the Osaka University Medical School Guidelines for the Care and Use of Laboratory Animals.

Quantitative real-time RT-PCR

Real-time RT-PCR was performed as previously described (*11*). Briefly, total RNA was isolated from cultured cells using the QuickGene RNA cultured cell HC kit (FUJIFILM, Tokyo, Japan) or from frozen liver using the RNeasy Plus Mini Kit (Qiagen, Valencia, CA) according to the manufacturer's instructions. The first-strand cDNA was synthesized from total RNA of each sample using the SuperScript™ First-Strand Synthesis System for RT-PCR (Invitrogen, Carlsbad, CA). The cDNAs were used as templates for individual PCR reactions using specific primer sets (Table I). PCR reactions were carried out using QuantiTect™ SYBR® Green PCR Kit (Qiagen). Cyclophilin A and β2-microglobulin were used for normalizing each expression data set for human and rat, respectively.

Enzyme-linked immunosorbent assays

Huh-7 cells were treated with DMSO, 1 μM GW7647 or 1 μM rosiglitazone for 3 days. The culture supernatants were harvested and the expression levels of hMBL were determined using a human MBL ELISA kit (R&D Systems, Minneapolis, MN). ELISA was carried out according to the manufacture's instruction and normalized to cell numbers measured by Cell Counting Kit-8 (Dojindo, Kumamoto, Japan).

Reporter gene assays

Reporter gene assays were performed as described previously (*11*). Briefly, HepG2 cells were seeded in 96-well plates 14–18 h before transfection. The cells were transfected with 80 ng of the reporter plasmid, 20 ng of phRL-TK (Promega, Madison, WI) and either 10 ng of pcDNA3, pcDNA3-hPPARα or pcDNA3-hPPARγ1 expression vector. Twenty-four hours after transfection, the cells were treated with DMSO, 100 nM GW7647 or 1 μM rosiglitazone. After 24 h, both firefly and *Renilla* luciferase activities were quantified using a Dual-Luciferase® Reporter Assay System (Promega).

Electrophoretic mobility-shift assays

Electrophoretic mobility-shift assays (EMSAs) were performed as described previously (*10*). Human PPARα and RXRα proteins were prepared using the IMPACT™-CN system (New England Biolabs, Ipswich, MA). Human PPARγ1 protein was synthesized *in vitro* using the TNT® Quick Coupled Transcription/Translation Systems (Promega). Supershift assays were performed using anti-PPARα (H0723, Perseus Proteomics, Tokyo, Japan), anti-PPARγ (A3409A, Perseus Proteomics), anti-RXRα (K8508, Perseus Proteomics) or anti-glyceraldehyde-3-phosphate dehydrogenase (GAPDH) (MAB374, Millipore, Billerica, MA) antibodies. In the competition studies, 10- or 100-fold molar excess of unlabelled double-stranded oligonucleotides were added to the reaction mixture. Double-stranded oligonucleotides composed of the following

sequences were used for the binding and competition assays: human MBL2 PPRE wild type, 5′-CAGATTGTAGGACAGAGG GCATGCTCG-3′, human MBL2 PPRE mutant, 5′-CAGATTGTA acAttGctGGaATGCTCG-3′ and rat acyl-CoA oxidase (ACO) PPRE, 5′-GCGGACCAGGACAAAGGTCACGTTC-3′.

Chromatin immunoprecipitation

Chromatin immunoprecipitation (ChIP) assays were performed as described previously (*10*). Antibodies for PPARα (H-98, Santa Cruz, Santa Cruz, CA), PPARγ (H-100, Santa Cruz), RXRα (D-20, Santa Cruz) or pre-immune rabbit IgG were used for the immunoprecipitation. The precipitated DNAs were analysed by PCR using the primers 5′-ATAGCCTGCACCCAGATTGT-3′ and 5′-AGAACA GCCCAACACGTACC-3′, which flanked the PPRE of the human MBL2 or primers 5′-ATGGTTGCCACTGGGGATCT-3′ and 5′-T GCCAAAGCCTAGGGGAAGA-3′, which are located about 6-kb upstream of the GAPDH promoter (negative control).

Statistical analysis

Data are expressed as the mean ± standard error of the mean (SEM). Statistical analyses were performed by Dunnett's multiple comparison test or Student's *t*-test using R for Mac OSX.

Results

PPARs induce human MBL2 expression in human hepatoma cell lines

Previously, to identify human PPAR responsive target genes, we established tightly Tet-regulated human hepatoblastoma cell lines that can be induced to express each human PPAR by the removal of tetracycline from the culture medium (HepG2-tet-off-hPPAR) (*10*). Subsequent microarray analyses indicated that human MBL2 was up-regulated by ligand-activated PPAR (GSE2699). To confirm whether PPAR modifies human MBL2 expression, we cultured HepG2-tet-off-hPPARα and hPPARγ1 cells in the presence or absence of Tet for 24 h, and then treated these cells with the PPAR ligands (GW7647 for PPARα or rosiglitazone for PPARγ) or DMSO (Control). Total RNA samples were prepared after a further 24 h incubation, and mRNA levels were determined by real-time RT-PCR. The human MBL2 mRNA expression was up-regulated by both the ligand-activated PPARα and PPARγ1 (Fig. 1A). To examine whether endogenous PPAR regulates the human MBL2 expression, we used human hepatoma cell line Huh-7. The expression levels of human MBL2 mRNA increased upon treatment with the PPAR ligands (Fig. 1B). Subsequently, we determined human MBL protein levels. An ELISA of culture supernatants showed that both GW7647 and rosiglitazone up-regulated the human MBL protein levels (Fig. 1C). These data indicate that endogenous PPARα and PPARγ induce the expression of the human MBL2 in Huh-7 cells.

PPARs activate the human MBL2 promoter activity via a PPRE

To investigate how PPARs affect human MBL2 expression, we analysed the 5′-flanking region of the human MBL2 gene. The human MBL2 promoter corresponding to the region −4942 bp to +68 bp was fused to the luciferase gene in the PGV-B basic vector to yield the reporter plasmid, termed hMBL2-Luc (Fig. 2A). We co-transfected either the PPAR expression plasmid (pcDNA3-hPPARα or pcDNA3-hPPARγ1) or the vector plasmid as a control together with the reporter plasmid into HepG2 cells. These cells were subsequently incubated with either ligand (GW7647 or rosiglitazone) or DMSO for 24 h and used for reporter gene assays. Ligand-activated PPARs induced the promoter activity of the human MBL2 reporter plasmid (hMBL2-Luc) to a level 5- to 17-fold higher than the control (PPAR + Ligand versus pcDNA3 + Control) (Fig. 2A). These results suggest that human MBL2 promoter is regulated by PPARs.

To identify the region within the human MBL2 promoter that confers transcriptional responsiveness to ligand-activated PPARs, we carried out 5′ deletion analyses. Although the induction of luciferase activity by PPARs was observed using five deletion constructs (hMBL2-3711, -2981, -1980, -1144 and -113), a further 5′ deletion construct (hMBL2-1) was no longer induced by PPARs (Fig. 2A). These results indicate that a functional PPRE is located in the region between −113 bp and −1 bp of the human MBL2 promoter. Indeed, we found a putative PPRE sequence at position −14 bp to −2 bp (Fig. 2B). To test whether this sequence is a functional PPRE, we measured the luciferase activity of the PPRE mutation construct (hMBL2-Luc (mut)). We found that mutation of this PPRE abolished the transcriptional activation of the human MBL2 promoter by PPARs (Fig. 2B). These results indicated that the −14 bp to −2 bp site in the human MBL2 promoter is a functional PPRE.

Binding analysis of PPARs to the human MBL2 promoter

To determine whether PPARs bind to this PPRE in the human MBL2 promoter, EMSAs were performed. The EMSAs revealed that PPARs could bind to this element in the presence of RXRα (Fig. 3A and C, lanes 3 and 4). This complex formation was competed by increasing amounts of the unlabelled self-competitor probe and rat ACO PPRE fragments, which is one of a PPAR binding element (*13*), but not by the mutated PPRE probe (Fig. 3A and C, lanes 5–10). No protein–DNA complex was observed when the mutated PPRE was used as a radiolabelled probe (Fig. 3A and C, lane 11). To confirm that this complex contains both PPARs and RXRα, we performed supershift experiments. Monoclonal antibodies against PPAR and RXRα yielded supershift bands (Fig. 3B and D, open arrowheads on lanes 4 and 6, respectively). As expected, a control antibody had no significant effect (Fig. 3B and D, lane 8).

To confirm that the PPARs/RXRα heterodimers bind to this PPRE in cells, we performed ChIP assays. HepG2-tet-off-hPPAR cells were treated with the PPAR ligands (GW7647 or rosiglitazone) for 2 h. These cells were subsequently used for ChIP assays. The co-precipitated DNA fragments were detected by PCR amplification. Specific amplification of the PPRE in the endogenous human MBL2 promoter was detected when antibody for PPARα, PPARγ or RXRα was used, but not when the pre-immune rabbit IgG was used (Fig. 4A and B, upper panel). In contrast, a

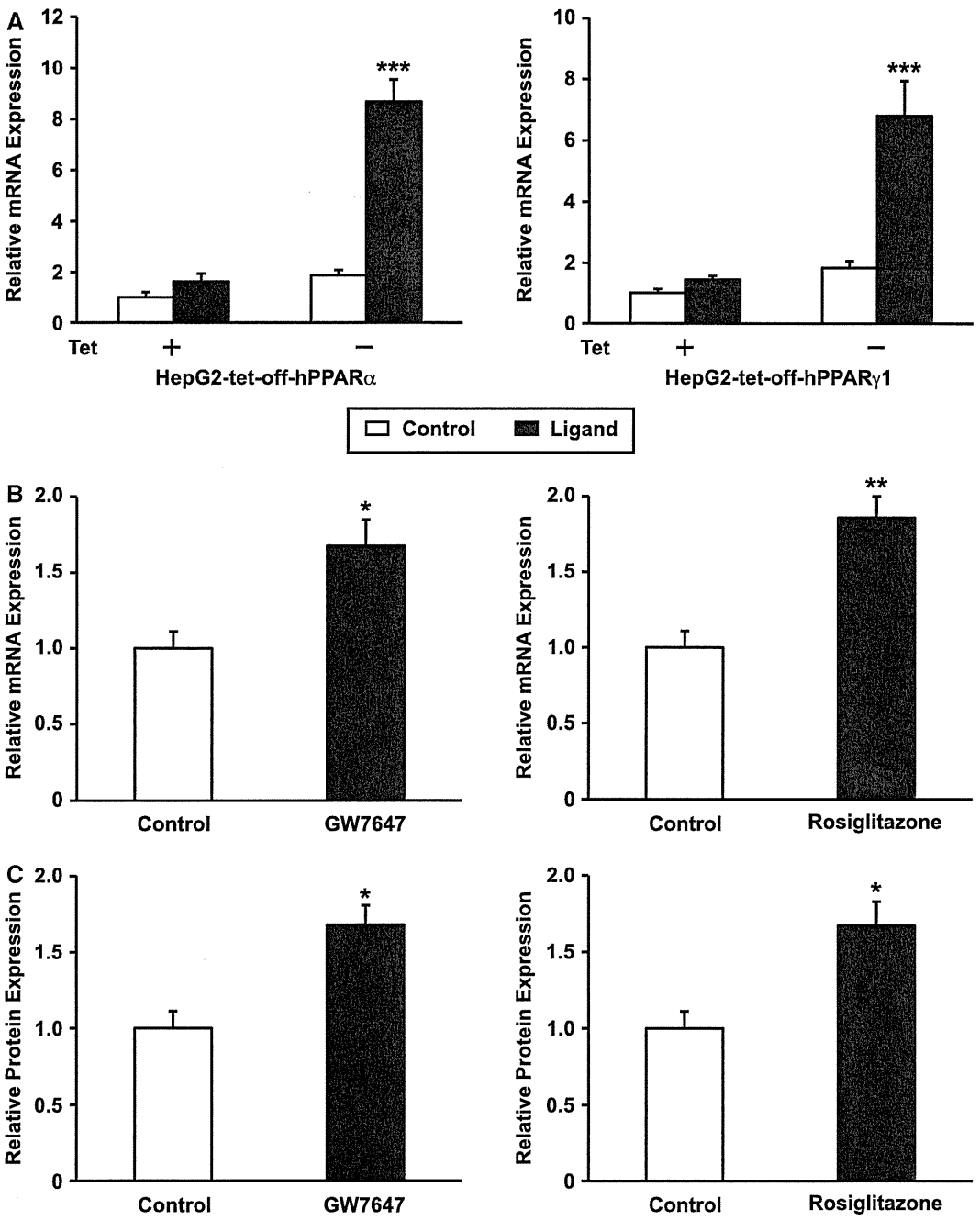

Fig. 1 Human MBL2 expression is regulated by PPARα and PPARγ in human hepatoma cells. (**A**) HepG2-tet-off-hPPAR cells were cultured in the presence (+) or absence (−) of Tet for 24 h. The cells were treated with PPAR ligand (1 μM GW7647 for PPARα or 1 μM rosiglitazone for PPARγ1) or DMSO (Control) for 24 h. Human MBL2 mRNA levels were measured by real-time RT-PCR and normalized to Cyclophilin A mRNA, relative to the control (presence of Tet with control) set as 1. Values are expressed as the mean ± SEM ($n = 3$). Significant differences of the values compared to the control were determined using Dunnett's test and are indicated by asterisks (***$P < 0.001$). (**B**) Huh-7 cells were treated with 1 μM GW7647, 1 μM rosiglitazone or DMSO (Control) for 48 h. Human MBL2 mRNA levels were measured by real-time RT-PCR and normalized to Cyclophilin A mRNA, relative to the control set as 1. Values are expressed as the mean ± SEM ($n = 3$). (**C**) Huh-7 cells were treated with 1 μM GW7647, 1 μM rosiglitazone or DMSO (Control) for 3 days. Human MBL protein in cell culture supernatants were measured by ELISA and normalize by number of cells. Values are expressed as the mean ± SEM ($n = 3$). Significant differences of the values compared to the control were determined using Student's *t*-test and are indicated by asterisks (*$P < 0.05$, **$P < 0.01$).

second set of primers for amplifying another genomic region ~6 kb upstream of the human GAPDH gene that was expected to interact with neither PPARs nor RXRα yielded a PCR product by using only the input DNA (Fig. 4A and B, lower panel). Taken together, these results indicate that PPARs and RXRα bind to this PPRE in the human MBL2 promoter.

Rat MBL2 gene expression levels is not regulated by PPAR ligand

Next, we examined whether treatment with PPAR ligand could regulate the MBL2 gene expression *in vivo*. Because the liver is the main site of expression for both PPARα and MBL2 (*1*, *14*), liver samples for RNA isolation were collected from rats treated with

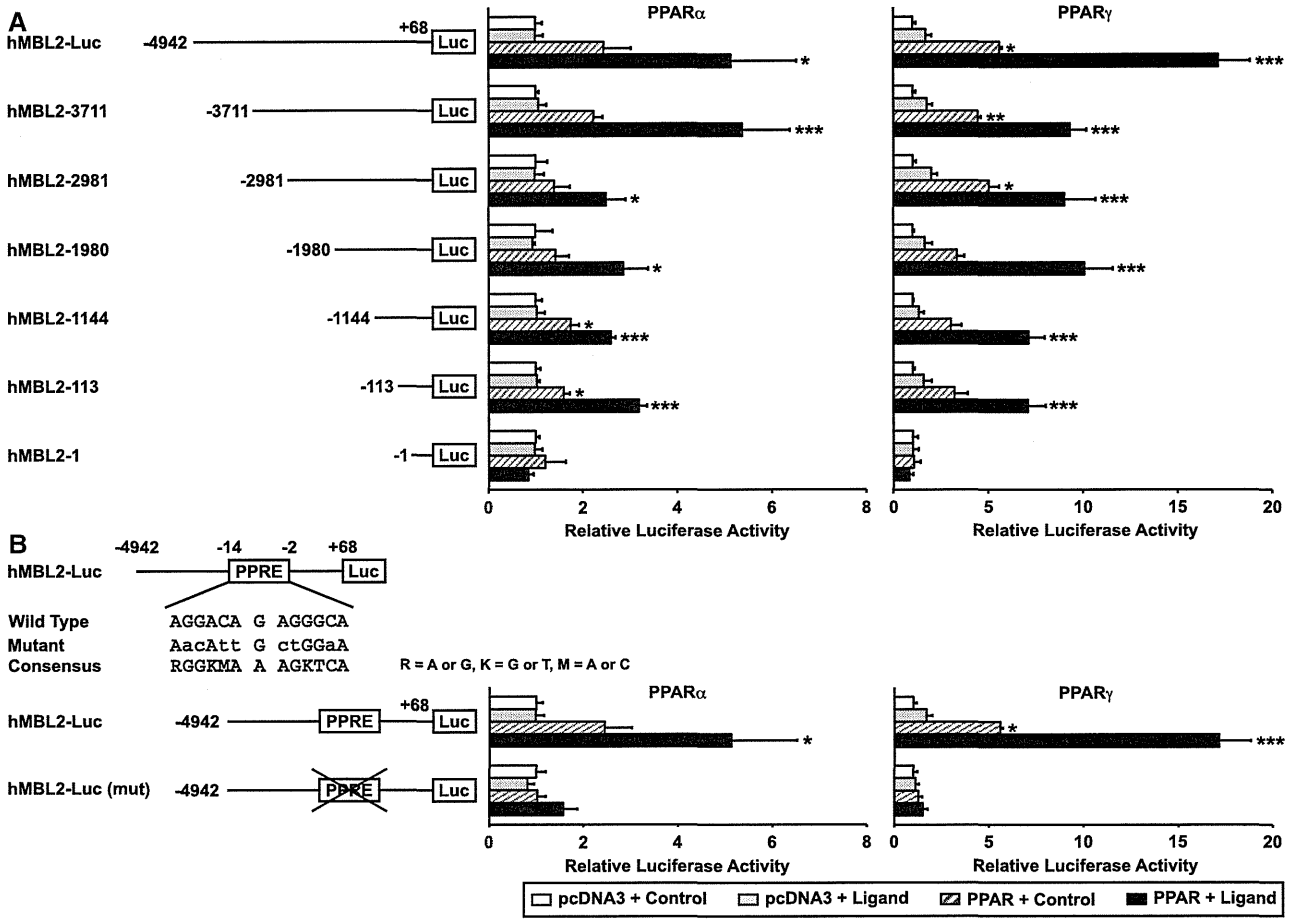

Fig. 2 PPARα and PPARγ modulate human MBL2 promoter activity via a PPRE. (**A**, **B**) Schematic representation of the human MBL2 promoter. Lower-case letters indicate mutations introduced in the potential PPRE. The number represents the positions relative to the transcription initiation site (+1) (*12*). HepG2 cells were co-transfected with the indicated reporter plasmids, phRL-TK and either pcDNA3, pcDNA3-hPPARα or pcDNA3-hPPARγ1. Transfected cells were treated with ligand (100 nM GW7647 or 1 μM rosiglitazone) or DMSO (Control) for 24 h. Luciferase activities from reporter plasmids were normalized to *Renilla* luciferase activities. Values are expressed as fold induction of the control set as 1. Values represent the mean ± SEM ($n = 3$). Significant differences of the values compared to the control were determined using Dunnett's test and are indicated by asterisks (*$P < 0.05$, **$P < 0.01$, ***$P < 0.001$).

either fenofibrate (a PPARα agonist) or vehicle alone for 4 days. In rat liver, fenofibrate induced a significant increase in the expression of ACO, which is a known rat PPARα target gene (*13*). However, the mRNA level of MBL2 was not affected in response to fenofibrate in rat liver (Fig. 5A). Furthermore, although the expression levels of ACO mRNA increased upon treatment with the PPARα ligand GW7647, MBL2 mRNA expression levels were not affected in rat H4IIE hepatoma cells (Fig. 5B). These data indicate that MBL2 mRNA expression was not affected by the PPARα ligand both *in vivo* in rat liver and *in vitro* in rat H4IIE hepatoma cells. In addition, MBL2 mRNA expression was not affected by the PPARγ ligand in H4IIE cells (Supplementary Fig. S1).

Species differences in response to PPAR

We wondered whether the lack of induction of MBL2 gene expression by PPAR ligand in rats was due to the absence of a functional PPRE in the rat MBL2 promoter. When the human and rat 5′-flanking regions upstream from the translation initiation codon (ATG) were aligned, three nucleotide differences were observed (Fig. 6A). To determine whether these nucleotide differences conferred species differences in the MBL2 gene expression in response to PPAR, we performed reporter gene assays. The human and rat MBL2 PPRE were cloned into the upstream region of the SV40 promoter driving luciferase reporter gene in the PGV-P2 vector. When we co-transfected this reporter plasmid (hMBL2-PPRE) with the PPAR expression plasmid in HepG2 cells, the reporter vector containing the human PPRE was effectively transcribed by ligand-activated PPARs (Fig. 6B, 2- to 4-fold higher than the control (PPAR + Ligand versus pcDNA3 + Control)). In contrast, no change in the transcriptional levels was observed when the reporter vector containing the rat DR1 (rMBL2-DR1) was used as a reporter plasmid (Fig. 6B). These data clearly indicate that only the human, but not the rat, MBL2 promoter contains a functional PPRE.

Discussion

MBL is a member of the collectin family and is important in innate immunity (*1*). However, little is

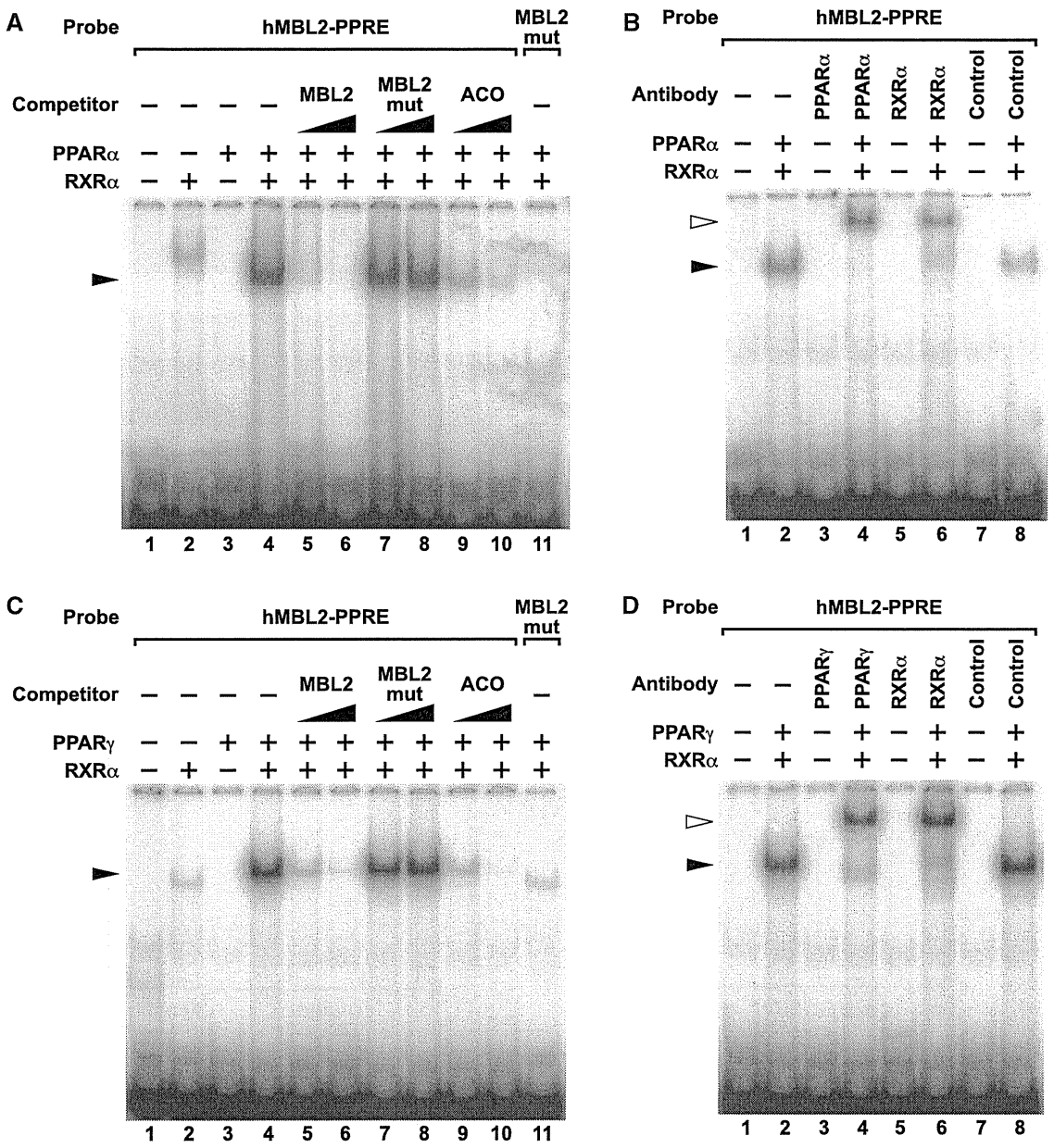

Fig. 3 PPARα and PPARγ bind to the PPRE of the human MBL2 gene. (A–D) EMSAs were performed with [^{32}P]-labelled human MBL2 PPRE (hMBL2-PPRE) or mutated human MBL2 PPRE (MBL2 mut) oligonucleotides in the presence of PPARα (A, B), PPARγ1 (C, D) and/or RXRα proteins. Unlabelled oligonucleotides (MBL2, MBL2 mut or ACO) were used at 10- or 100-fold molar excess to the labelled probe to perform competition assays. Supershift experiments were carried out using anti-PPARα (B), anti-PPARγ (D), anti-RXRα or anti-GAPDH (Control) antibodies. Closed and open arrowheads indicate the specific shift bands and the supershift bands, respectively.

known about transcription factors that regulate human MBL2 promoter activity (*5*). In this study, we showed that PPARs up-regulate the expression of human, but not rat, MBL2. A reporter analysis revealed that PPRE exists in the human MBL2 promoter and PPARs can directly bind to this region. These results indicate that human MBL2 expression is regulated by PPARs via a PPRE.

In recent years, Fraser and Tenner (*4*) showed that MBL bound to oxidized (atherogenic) low-density lipoprotein and increased cholesterol efflux in human macrophages. Mechanisms governing the removal of modified lipoproteins are critical to the suppression of atherosclerosis. In this viewpoint, it is important to know whether the regulation of MBL2 expression by PPARs occurs in normal hepatocyte. Recently, Rakhshandehroo *et al.* (*16*) showed that MBL2 mRNA expression levels were up-regulated by Wy-14643 in primary human hepatocytes and plasma MBL levels were increased by fenofibrate in humans. Thus, PPAR ligands increasing the amount of MBL might be attractive candidates for anti-atherogenic therapy.

On the other hand, we showed that rat MBL2 expression levels were unaffected by PPAR ligands. Fibrates also could not induce the mouse MBL2 gene expression (*16*). These data suggest that there is a species difference in regulation of MBL2 gene expression

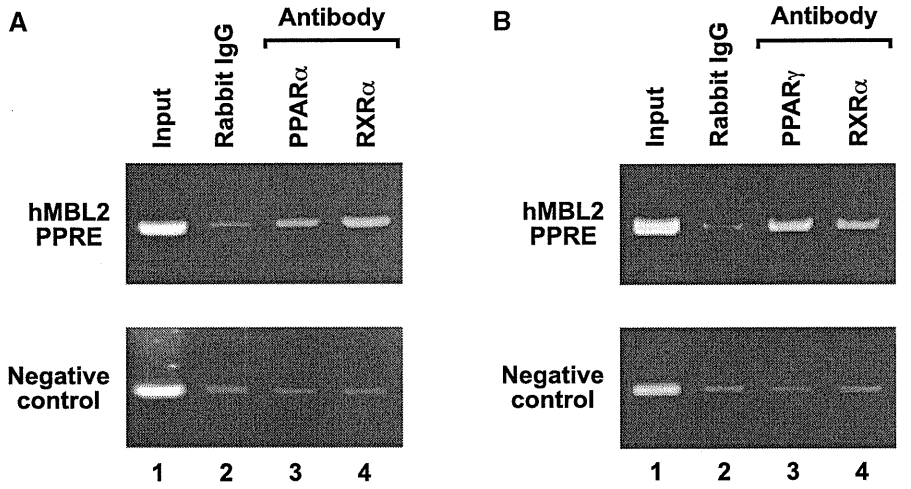

Fig. 4 ChIP assays revealed that PPARα and PPARγ bind to the PPRE of the human MBL2 gene. (**A**, **B**) HepG2-tet-off-hPPAR cells were treated with PPAR ligand (1 μM GW7647 or 1 μM rosiglitazone) and processed for ChIP assays. Soluble chromatin was immunoprecipitated with pre-immune rabbit IgG, anti-PPARα antibody (A), anti-PPARγ antibody (B) or anti-RXRα antibody. Immunoprecipitates were subjected to PCR with a primer-pair specific to the human MBL2 promoter (upper). As a negative control, a second set of primers was used to amplify another genomic region that was expected to interact with neither PPARs nor RXRα (lower).

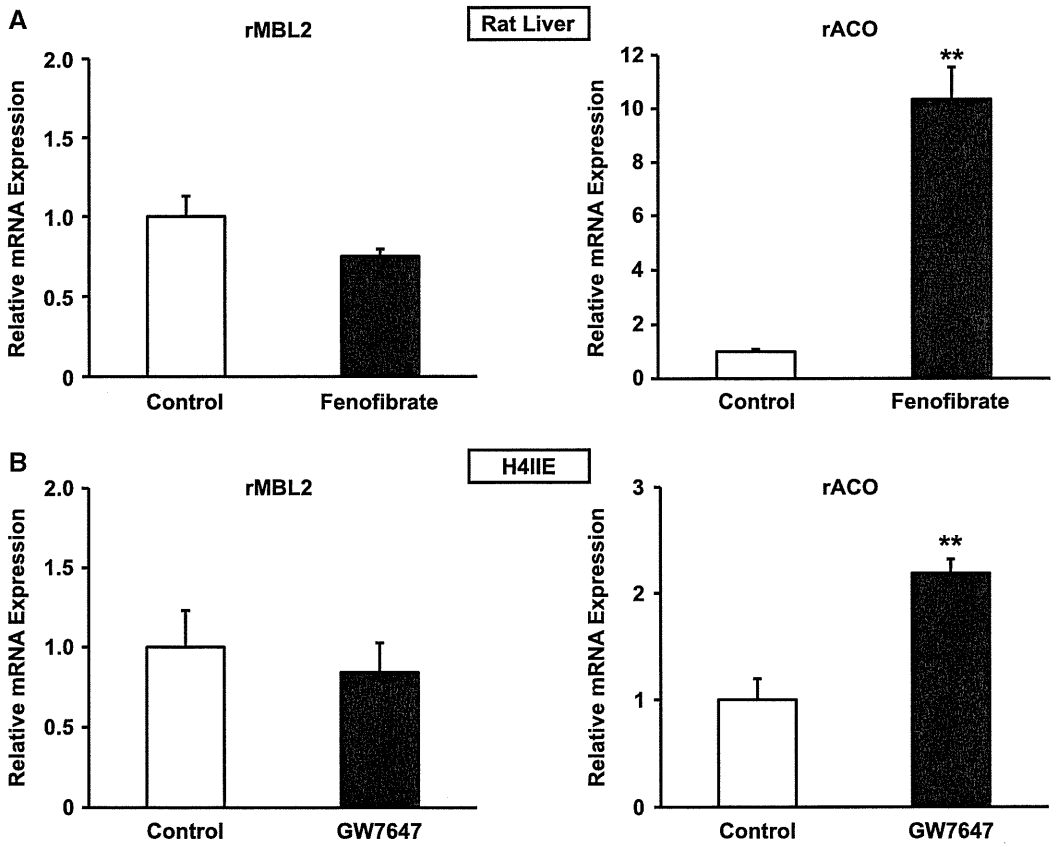

Fig. 5 Rat MBL2 mRNA expression levels were not affected by PPAR. (**A**) Fenofibrate (400 mg/kg) were orally administrated to rat for 4 days. MBL2 and ACO mRNA levels in the liver of rat were measured by real-time RT-PCR and normalized to β2-microglobulin mRNA, relative to the control set as 1. Values are expressed as the mean ± SEM ($n = 3$). (**B**) H4IIE cells were treated with 1 μM GW7647 or DMSO (Control) for 48 h. Rat MBL2 and ACO mRNA levels were measured by real-time RT-PCR and normalized to β2-microglobulin mRNA, relative to the control set as 1. Values are expressed as the mean ± SEM ($n = 3$). Significant differences of the values compared to the control were determined using Student's *t*-test and are indicated by asterisks (**$P < 0.01$).

by PPARs between humans and rodents. Interestingly, when the human, rat and mouse 5′-flanking regions upstream from the translation initiation codon were aligned, three nucleotide differences were observed in the PPRE (Fig. 6A, Supplementary Fig. S2). Indeed, rat DR1 did not affect the reporter activity (Fig. 6B). A similar pattern was observed in the regulation of apolipoprotein A-I gene. The absence of induction of

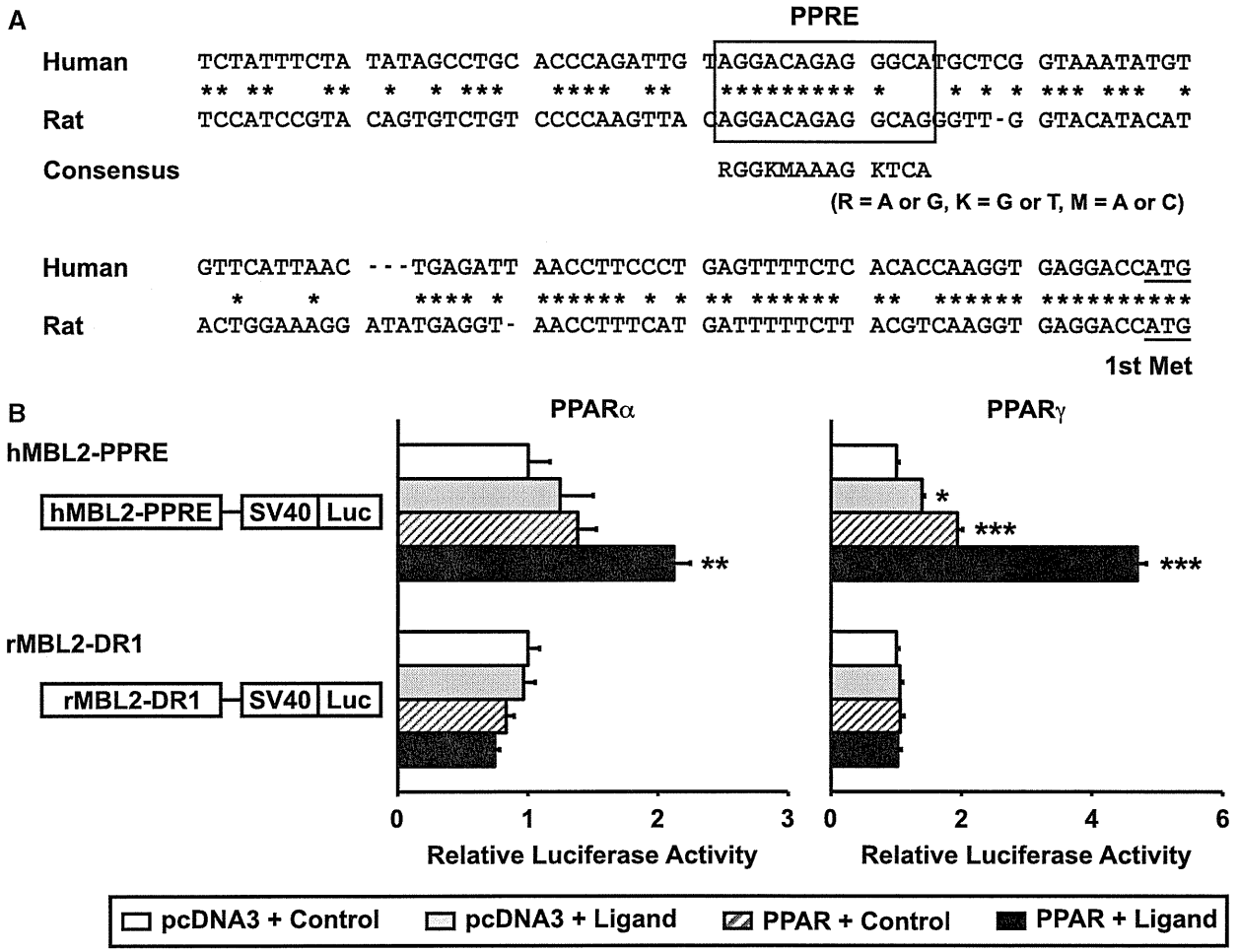

Fig. 6 PPARα and PPARγ activate the human, but not rat, MBL2-PPRE. (**A**) Comparison of the genomic sequence upstream of the human and rat MBL2 genes (*12*, *15*). Nucleotides identical between the human and rat sequence are indicated by asterisks. The position of the human MBL2 PPRE is indicated by box. Solid line below the sequence indicates the translation initiation codon ATG. (**B**) HepG2 cells were co-transfected with the indicated reporter plasmids, phRL-TK and either pcDNA3, pcDNA3-hPPARα or pcDNA3-hPPARγ1. Transfected cells were treated with ligand (100 nM GW7647 for PPARα or 1 μM rosiglitazone for PPARγ) or DMSO (Control) for 24 h and the cells were used for reporter gene assays. Luciferase activities from reporter plasmids were normalized to *Renilla* luciferase activities. Values are expressed as fold induction of the control (the value when pcDNA3 was transfected and treated with DMSO) set as 1. Values represent the mean ± SEM ($n = 3$). Significant differences of the values compared to the control were determined using Dunnett's test and are indicated by asterisks ($^{*}P < 0.05$, $^{**}P < 0.01$, $^{***}P < 0.001$).

rat apolipoprotein A-I gene expression by fibrates is due to three nucleotide differences between the rat and the human apolipoprotein A-I PPRE (*17*). Thus, although further investigations are required, the species differences in response to PPAR could be due in part to sequence-specific differences in the PPRE in the promoter region of MBL2.

In conclusion, we describe for the first time that the human, but not the rat, MBL2 promoter contains a functional PPRE. Namely, human MBL2 is a direct target gene of PPARs. This novel finding that human MBL2 expression is regulated by PPAR suggests a potential therapeutic effect of PPAR ligands in the treatment of atherosclerosis.

Supplementary Data

Supplementary Data are available at *JB* Online.

Funding

This work was supported by Grant-in-Aid for Young Scientists (B) and the Global COE Program 'in silico medicine' at Osaka University.

Conflict of interest

None declared.

References

1. Kawasaki, T. (1999) Structure and biology of mannan-binding protein, MBP, an important component of innate immunity. *Biochim. Biophys. Acta* **1473**, 186–195
2. Madsen, H.O., Videm, V., Svejgaard, A., Svennevig, J.L., and Garred, P. (1998) Association of mannose-binding-lectin deficiency with severe atherosclerosis. *Lancet* **352**, 959–960
3. Matthijsen, R.A., de Winther, M.P., Kuipers, D., van der Made, I., Weber, C., Herias, M.V., Gijbels, M.J., and Buurman, W.A. (2009) Macrophage-specific